An Underactuated Flexible Instrument for Single Incision Laparoscopic Surgery

A Thesis Presented for the

Master of Science

Degree

The University of Tennessee, Knoxville

Zhe Su

May 2019

© by Zhe Su, 2019
All Rights Reserved.

Acknowledgements

Foremost, I would like to express my sincere gratitude to my advisor Dr. Jindong Tan for all his support of my study and research, for his patience, motivation, enthusiasm, and immense knowledge. His guidance helped me in all the time of research and this thesis and I think I've become a better person with his mentoring. Also I would like to thank my committee member professors, Dr. Hamel and Dr. Rucker. They not only taught me fascinating courses but also gave me kind encouragement, they are ones of the wisest men I've ever known. I would like to thank The University of Tennessee Knoxville for these wonderful, educational and unforgettable years of education. Without these experience I could never be the person I am now.

Abstract

More and more patients and surgeons have switched from open surgery to minimally invasive surgery over these years. This exciting advancement has brought massive benefits to patients. Researchers and institutions have proposed robot assisted surgery which combines the advantage of developed robot system and human experience. This thesis reviews state of the art in this area and analyze some advanced surgical instrument for single incision laparoscopic instrument, then propose a design of robotic instrument for single incision laparoscopic surgery which can be integrated with collaborative robot manipulator to construct a surgical robot system.

Single-incision laparoscopic surgery (SILS) has its own features and advantages compare to other minimally invasive surgery techniques which also lead to special design requirements for SILS instruments, among which increased flexibility compare to multi-incision surgery instruments is an important part. So we want to design a robotic surgical instrument that has increased flexibility compare to traditional instruments for other MIS techniques. As a laparoscopic robotic instrument compactness and light weight are also our considerations.

Single incision laparoscopic surgery (SILS) inserts multiple instruments and laparoscopes through a single trocar which reduces trauma. But this improvement for patients caused difficulty in operation because of instruments triangulation,

laparoscope field-of-view, etc. That brings up our challenges in designing a robotic instruments. Designing a highly flexible robotic instrument that provides sufficient workspace and good triangulation in order to relieve the difficulties introduced by narrow instrument trocars.

We want to implement a highly recognized surgical instrument with a designed robotic instrument actuation pack. These two parts compose a robotic surgical instrument for single incision laparoscopic surgery. And we want to analyze the performance and viability of our design approach for SILS application.

Table of Contents

1 Introduction **1**

1.1 Disclaimer 1

1.2 Background of surgical techniques 2

1.3 Motivation and Design Goals 3

1.3.1 Motivation 4

1.3.2 Design Goals 4

2 State-of-the-Art **8**

2.1 Open Surgery and MIS Instrumentation 8

2.2 State of the Art Study 10

2.2.1 Surgical Robotic Systems for MIS 10

2.2.2 Laparoscopic Instruments Designs 12

2.2.3 The Advantages of Underactuated Multi-Joint Flexible Robot 14

3 Design of Surgical Instrument for SILS **16**

3.1 Overall Design Plan 16

3.2 Surgical Instrument Selection and Its Kinematics 17

3.2.1 Instrument Selection: SILS™by **Medtronic** 18

3.2.2 Kinematics of Multi-joint Flexible Robot 20

3.3 Mechanical Design of Actuation Pack 27

3.3.1 Mechanical Design 28

3.3.2 Actuator Space Kinematics Mapping 31

4 Actuation Pack Hardware Design **45**
4.1 Overall Structure 45
4.2 Mechanical Design Annotation 47
4.2.1 Flexible Instrument Shaft 47
4.2.2 Shaft Holder/ Tendon Plate Shell 48
4.2.3 Tendon Plate 48
4.2.4 Base and External Support 51

5 Results and Simulation **53**
5.1 Instrument Assembly 53
5.2 Simulation and Analysis 53

6 Conclusion **61**

Bibliography **64**

A Summary of Equations **69**
A.1 Cartesian 70

Vita **76**

Nomenclature

α	Articulation Angle of Servo-I about X Axis on Cable Knob
β	Articulation Angle of Servo-II about Y Axis on Cable Knob
ϕ	Bending Direction
θ	Articulation Angle of Each Joint
φ	Total Bending Direction
ϑ	Total Bending Angle
D	Outer Diameter of Flexible Joints, Shaft Diameter
d	Distance between Opposite Tendons
H	Height of Each Joint Body
h_0	Height of the Gap between Joints at Initial Position
h_l	Height of the Gap on the Left between Joints after Articulation in 2D
h_r	Height of the Gap on the right between Joints after Articulation in 2D
L_i	Driving Tendon Lengths
L_i'	Virtual Tendon Length

N	Number of Joints
N_f	Number of Flexible Joints
T_{knob}	Transformation Matrix of Cable Knob Articulation
W_i	Driving Tendon Locations
X	x Coordinate of End-Effector
x	x Coordinate of End-Effector in XOZ Plane
y	y Coordinate of End-Effector
Z	z Coordinate of End-Effector
z	z Coordinate of End-Effector in XOZ Plane

Chapter 1

Introduction

The core content of this thesis presents a surgical robot for single incision laparoscopic surgery and exploration parallel manipulator application in under-actuated mechanism control. And to make our design fit for single incision laparoscopic application we need to review the evolution of minimally invasive surgical techniques, and analyze some major differences between SILS and the rest of surgical techniques so we can design our surgical instrument that will fit for single incision surgery applications. Our goal is to design a robotic surgical instrument that features enhanced flexibility. In the mean time we will try to reduce the cost and weight of the surgical robot in order two give the system more payload capacity.

1.1 Disclaimer

I hereby declare that this thesis is my own and autonomous work. All sources and aids used have been indicated as such. All texts either quoted directly or paraphrased have been indicated by in-text citations. Full bibliographic details are given in the reference list which also contains internet sources containing URL and access date. This work has not been submitted to any other examination authority.

1.2 Background of surgical techniques

Surgeries has evolved from open surgery to modern minimally invasive surgery. The size of the incisions made on patients' bodies have been reduced massively. Traditional open surgery requires a large open incision near the surgery site, this causes problems such as large amount of blood loss, high risk of infection and cosmetic issues. As surgical techniques evolved, minimally invasive surgery has been a main stream technique for cardiac surgery, colorectal surgery, gynecologic surgery, thoracic surgery, etc. Minimally invasive surgery only requires one or a few small incisions to be made on patients' abdomen instead of large incisions. And a few laparoscopic surgical instruments are inserted through those small incisions to reach and operate on the surgical site.

This great improvement has brought significant improvement in patient benefits such as pain management, post-surgery recovery time and cosmetic benefits. The benefits of MIS are the reason surgeons and patients chose MIS over open surgery, but they also introduced even more technical difficulties into operation resulting in extended operation time, surgeon exhaustion and longer anesthetization duration.

Recent years it has come to the era of robot assisted surgery due to the development of robotic technology. With the help of modern technology surgeons with robotic surgical techniques training are able to perform using surgical robots, replacing manual laparoscopic tools with flexible and miniature robot hands that can be manipulated remotely with various controllers. Nowadays surgeons can operate much more longer, and the success rate of MIS has improved.

We generally concluded how minimally invasive surgery works and the benefits it brings, we can introduce some different kinds of minimally invasive surgery techniques. The most common laparoscopic surgical applications are performed by making multiple incisions on patient's abdomen through which traditional

laparoscopic tools are inserted. Another kind of laparoscopic surgery is single-incision laparoscopic surgery. Single-incision laparoscopic surgery aims to reduce the number of incisions made during surgery. Typically surgeon open a 5 cm incision on patient's abdomen, SILS features a multi-port trocar which is inserted through this incision. This trocar has several port that allows endoscopes and instruments to be inserted. This definitely reduced the number of traumas, but there are limits. For example since instruments are inserted through the same trocar, the chance of instrument collision goes higher. Another kind of laparoscopic surgery is natural orifice transluminal endoscopic surgery also known as NOTES. The idea of NOTES transfers surgical incision in to orifice on human body like Esophagus and rectum so no scar will be left where can be seen. Of course this technique brings even more cosmetic benefits to the patients, but it certainly requires more advanced surgical robots than single port laparoscopic surgery. Robot designs for NOTES are more complicated than laparoscopic instruments because most conceptual designs are designed to be fully inserted which adds the complexity of robot design and difficulty surgery. Our design is for common laparoscopic surgery and single-incision laparoscopic surgery.

1.3 Motivation and Design Goals

In this section we will discuss the motivation of designing a surgical robotic instrument for SILS and our design goals. We will explain why SILS is our targeted area given the unique features of SILS. And we want to present our design goals of this thesis to provide a clear idea of what we want to achieve.

1.3.1 Motivation

As we discussed in section 1.2, MIS which benefits from the assistance of robotic technology has been changing medical care and it has been accepted by people including patients and doctors. Robotic and Automation technology can make up to the difficulties of operating within a narrow surgical site through one or more small surgical incisions, however manual laparoscopic surgery still remains the majority of MIS. This is because the higher cost of laparoscopic surgery with large-scale surgical robot. Another fact we can't ignore is that manual laparoscopic tools have already been in the hospitals and they are quite popular in most of the smaller surgeries. And note that every surgeon has been trained for manual laparoscopic surgery, but not all of the surgeons has access to expensive surgical robots.

Manual laparoscopic tools are popular because they are cheaper and has the same capabilities in terms of flexibility and dexterity, the major disadvantage of manual instruments is maneuverability. Without the integration of automation technology manipulation of most of the manual instruments could get tricky depending on the structure of manual laparoscopic instrument.

So we want to build a laparoscopic surgical robot that could utilize the SILS laparoscopic instrument, and together they compose a robotic laparoscopic instrument. This way we can combine the advantages of SILS laparoscopic instrument and robotic technology. We can provide same level of flexibility and dexterity as surgical robots and make a surgical instrument that could be applied to single incision laparoscopic instrument.

1.3.2 Design Goals

Our overall goal of this thesis is to design a robotic laparoscopic instrument for single incision laparoscopic surgery. To be more specific, meeting requirements of single incision laparoscopic instruments with enhanced dexterity and flexibility with lower cost in a reduced weight and compact pack. Flexibility in this case

means sufficient flexibility, isotropy and workspace inside patients' abdomen cavity. The reasons enhanced flexibility is required are related to the nature of SILS, which is caused by its unique surgical incision. For most surgical robots they have more than 6 DoFs which is sufficient or redundant for most 3D space tasks, but SILS instrument insertion is through a surgical trocar which binds some of the DoFs of surgical robot as shown in Fig. 1.1. In order to re-endow sufficient DoFs at surgical sites most research teams took an approach which adds extra flexibility on instrument wrist as we discussed before. Among all the works, we identify multi-joint flexible robot as a unique one that has the potential of being developed into a high-performance laparoscopic instrument because it has the features that suits SILS instruments.

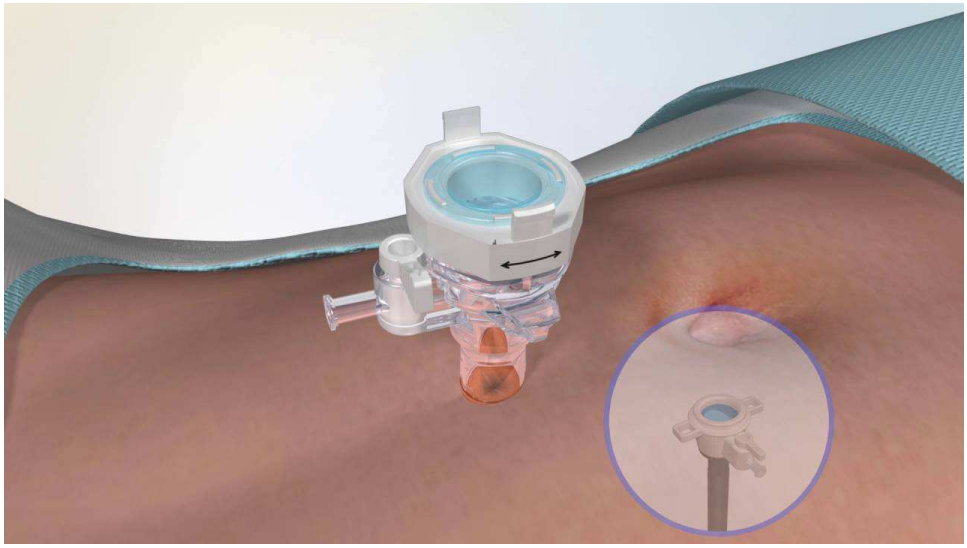

Figure 1.1: Trocar Placement in Single-Incision Abdominal surgery

To achieve this overall goal of ours, there are two main steps, surgical instrument and actuation pack design. The first step serves the purpose of achieving flexibility and stability under external interaction in single incision laparoscopic surgery. While we want to find the balance between control performance and system weight.

As we stated before, flexibility requirement of surgical instruments for minimally invasive surgery is increasing with the reduction in the total number of artificial incisions. As shown in Fig. 1.2, the instruments on the right are more suitable for single incision laparoscopic surgery Pourghodrat et al. (2017) because the are capable of providing triangulation with longer flexible part on the distal end of the instruments.

Figure 1.2: Surgical Instruments

According to **Intuitive Surgical**, thousands of hospitals have installed **Da Vinci Si** or **Da Vinci X** surgical robot systems. Even they have proven themselves reliable and proficient it is very hard to ignore the high cost of surgical robots not limited to **Da Vinci** products. And many hospitals in the U.S still couldn't install them and we have reason to believe the cost of surgical robot systems hasn't been helping popularize surgical robots. Typically the more flexible a surgical instrument is, the more expensive it is more possibly to be. Countless patients could enjoy the benefits of a low cost surgical robot so this thesis wants to show that robotic surgical robot can be cheaper without losing its flexibility. We want to claim first

that underactuated multi-joint flexible robot is very suitable for designing robotic surgical instrument for SILS which will be verified in later sections, we will design a surgical instrument with this structure. We need a instrument structure that is composed by a number of flexible joints that are driven by two pairs of tendons that are connected to the distal joint. And we will design an actuation pack with simple structure that drives the tendons.

With a suitable instrument the surgical tasks can be executed correctly if the control mechanism is designed correctly. There are designs that control this kind of instrument well. But we want to reduced the system weight by reducing the number of actuators used. And this is what brought us to parallel mechanism. Further design details are presented in later chapters. And we will analyze how well our actuation pack serves our purposes.

Chapter 2

State-of-the-Art

When establishing an design idea or searching for a valuable study subject, it is essential that we have a thorough knowledge of state of the art. Outstanding works have been established by other group. They all have their excellence in one or more area but their approaches and their motivation aren't always the same, on the contrary they of ten vary a lot. But they are all great reference and provide us guidance on our work. In this chapter, we will review state of the art of surgical and robotic surgical technology and discover the initial motivation of our idea.

2.1 Open Surgery and MIS Instrumentation

There are many designs and innovations that aim to improve the maneuverability and surgical outcome which helps both surgeons and patients. But first we need to focus on the differences in instrumentation of open surgery and MIS. We picked three genres of instruments as shown in Fig. 2.1. We can see the differences between instruments for open surgery and MIS are instrument handle design and the long thin shaft on MIS tools. Because surgeons don't have a large open surgical site MIS instruments have to manipulate end-effectors remotely through a remote handle which drives the gripper through different mechanism inside the instrument shaft while open surgery don't have to go through this trouble. This

is mainly caused by the small incision which great constrain sight, the range of motion of the instrument as well as surgeon's hands.

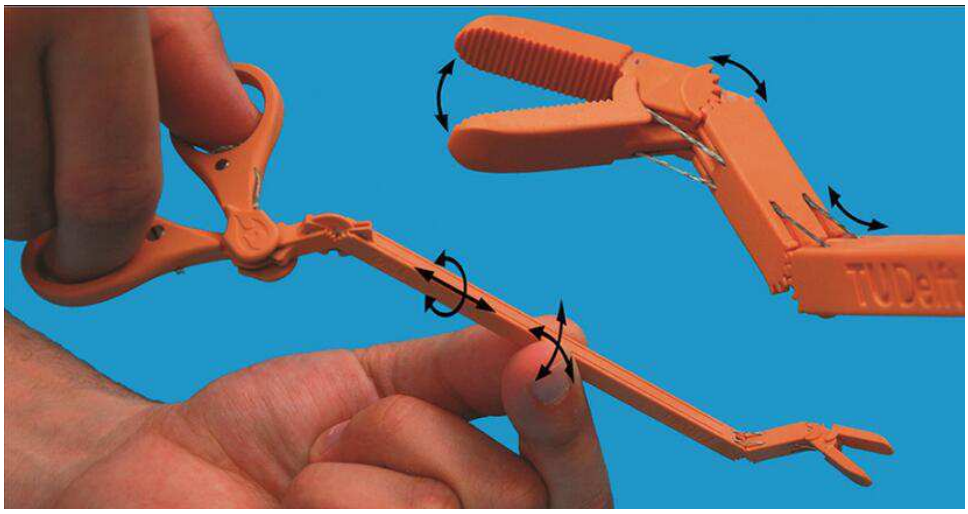

Figure 2.1: An Example of Instrument for Open Surgery, MIS and SILS

As in Fig. 2.1, the instrument on the right is Dragon Flex by Jelínek et al. (2014), it is an example of surgical instrument suitable for SILS. Same as the instrument for MIS, the DraonFlex allows remote operation by having a long shaft which allows the gripper operation handle that controls the end-effector through cable and gear structure locate on the shaft. But different from instrument for MIS it requires larger range of motion on the instrument wrist in order to expand workspace and enhance its triangulation. DragonFlex can represent most of instruments designed for SILS, they are all required to have a flexible instrument wrist in order to overcome the constraint introduced by the surgical incision, especially when multiple instruments are inserted through a single trocar. With a flexible wrist surgeons can benefit from a larger workspace, better triangulation which allows more complicated operation and wide field of view.

2.2 State of the Art Study

This part we will study some of the modern surgical robots, and some innovation on surgical instruments for MIS and SILS. Then we will specifically discuss the kind of instrument structure we picked for our design, the Underactuated Multi-Joint Flexible Robot.

2.2.1 Surgical Robotic Systems for MIS

Robot has been elevating human life in many areas like massive production, precision handling and multi-tasking. As we discussed laparoscopic surgery can be time consuming and exhausting for surgeons, so many research teams around the word developed surgical robot systems. Da Vinci surgical robot has been assisting surgeon in laparoscopic surgeries for many years, and it was well recognized by both surgeons and patients, in the year of 2012 over 40,000 surgeries were performed with the help of Da Vinci surgical robot Tan et al. (2016). But this famous surgical robot has some issues, high cost is considered to be the most unacceptable, not to mention that there are already surgical instrument designs that improved the performance. So we will introduce more surgical robot systems that has fixed some issues or improved the performance of Da Vinci.

Leonard et al. (2014) want to shorten the time of suturing in laparoscopic surgery, so they developed an automatic suturing robot. Their robot system is called "Smart Tissue Anastomosis Robot", also known as "STAR". It consists of a robot manipulator, a suturing tool and a surgeon interface. It can automatically identify the trauma or the incision and plan the positions of each stitch using computer vision technology. Of course surgeon can tell the position of the trauma and positions of each stitch to the robot through a robot surgeon interface. And the manipulator provides global positioning and point the instrument to the planned position of stitches. The instrument Leonard et al. (2014) has been introduced

above, it can guide the needle but it still needs cooperation of an assistant because it cannot make a knot. But according to their experimental results the robot has good positioning accuracy and greatly shortened operation time. Lee et al. (2014) developed a master-slave surgical robot. It has two components, the first is the surgical instrument introduced in Lee et al. (2014), the other component is a master robot with six degees of freedom force feed back. The master robot consists of seven degree of freedom, three of which at the wrist of the master robot are used to map orientation of the surgeon hand to the instrument tip, another three at the shoulder of the master robot are used to map the position, another one is used to map the motion of gripper. Also each degree of freedom has a feedback motor installed. This surgical robot system has great positioning accuracy and those feedback motors can give surgeon a good sense of environmental forces. Lum et al. (2009) developed the first generation of the RAVEN surgical robot, the RAVEN Surgical Robot consists of three main pieces: the patient site, the surgeon site and a network connecting the two Lum et al. (2009). The patient site is the surgical instrument which is constructed by mounting a instrument shaft to a three DoF instrument base. And the instrument is mounted on a 7 DoF serial robot manipulator. The surgeon site was developed to be low cost and portable, a choice that allows for easier tele-surgical collaboration. It consists of two PHANToM Omni devices Silva et al. (2009), a foot-pedal, a graphical interface which the surgeon can obtain visual signal of the surgical site with, and a video input of the surgical site. This system has same function blocks as the Da Vinci robot, but built in a low-cost way. And later Hannaford et al. (2013) developed a new version of the RAVEN robot, they improved the performance of the surgical instrument by adding an articulated wrist thus improved workspace and isotropy. Now RAVEN II surgical robot is considered another success in the area of surgical robotics, many research groups chose RAVEN II as their experiment platform. Another design worth mentioning is developed by A. Seneci et al. (2016) because it has similar structure as the RAVEN II robot and also features high performance and

fast assembly. This system has two main parts, the first is a fast assembly surgical instrument as we introduced in instrument designs A. Seneci et al. (2016). It has a custom designed docking mechanism that allows it to be easily docked to a 6 DoF robot manipulator which is the second physical part that construct the system. It is worth mentioning that both the instrument and the manipulator have many 3-D printed parts thus they can be assembled very fast. Also there are merchandised haptic feedback master controller like Omega 7 by ForceDimension, it measure surgeons hand position and orientation with multiple motors and encoders. It also has seven degree of freedom force feedback.

2.2.2 Laparoscopic Instruments Designs

Shang et al. (2017) highly flexible surgical instruments. The way they achieve this is constructing a 2 DoF bending wrist by a multi-slider linkage mechanism. This idea has inspired many more articulated tip instruments. A more extreme way of implementing multi-DoF is developed by Piccigallo et al. (2010) developed a surgical robot that place two six DoF anthropomorphic arm into the abdomen cavity and operate. Those robot arms are inserted through an incision of about 30-35mm. Joint 1 and 2 of each arm is cable driven and other four joints are driven by thin-diameter DC motors. This robot provides about 10 N of gripping force and a angular velocity of $2\pi/s$ to perform surgical tasks and follow surgeon's motion. Lee et al. (2016) developed a laparoscopic tool which features force sensing capability. This tool incorporated three force sensors, one of which is located at the instrument wrist, the other two are located at the base. Those sensors sense the environmental force at the one DoF wrist and two jaws. Jaws and wrist of this instrument are driven by pulleys. According to their experimental results shows that environmental force can be measured accurately. But the flexibility provided by this instrument is not as good as others and motion of wrist and

jaws are coupled by pulleys. Pulleys cannot provide sufficient gripping force. Haraguchi et al. (2015) developed a pneumatically driven surgical instrument to resolve the issue that tendon mechanism cannot provide much gripping force. The forceps of the instrument has flexible joints on the instrument wrist which is actuated by axial motions of super-elastic cables. And the continuous mechanism at instrument wrist is actuated by four pneumatic cylinders to guarantee the wrist can rotate in 360 degrees thus the motion between forceps and wrist are decoupled. And the force sensing is achieved by using pressure sensor to measure the air pressure in pneumatic cylinders thus can estimate the environmental force, the experimental results showed that this instrument can estimate external force accurately. Lee et al. (2014) developed a master-slave structure robotic surgical system that features a tendon driven instrument. The instrument tip has four degrees of freedom, one shaft rotation, on at the wrist, two separate jaws. The tendons used to drive wrist and jaws are inserted through a hole on a drum which is placed at the proximal end of the instrument. This drum is mechanically linked to the motor by another tendon, so the torque output of the motor is passed to the drum and rotation of the tendon used to drive jaws and wrist rotate with the drum. External force is estimated through current information of the motor. To decouple the motion of shaft and wrist, another motor is located at the distal side of the instrument to provide rotational actuation to the whole body so the wrist's motion is decoupled from shaft rotation. Hannaford et al. (2013) designed RAVEN II surgical robot. The instrument of RAVEN II consists of a gripper and 3 DoF manipulator to provide global positioning and expend workspace. The gripper used same tendon driven mechanism as the EndoWrist of the Da Vinci robot, it has a rotating wrist and two jaws. And the 3 DoF manipulator consists of three revolute joints. Most surgeries need two instruments, so the common configuration of RAVEN II consists of two instruments, note that the left and right instruments including their placement arms have different poses because they are on different sides of the patient. Raven II system achieved great performance, but

it still have issues like motion coupling, gripping force and tendon slipping. Up to this point all designs mentioned are either single-use or can be used for limited times. A. Seneci et al. (2016) designed a instrument with replaceable gripper and shaft with 3D-Printing technology. Application of 3D-Printing great reduce the time of design iteration and time of assembly. This instrument consists of a holding base that contains motors, electric boards force sensors and connection hooks, and the shaft has two flexible joints on the wrist and one flexible jaw. Through the connection hooks we can easily attach or detach the shaft to or from the holding base. Thus we can replace the shaft after a surgery instead of replacing the whole instrument. Also it can measure the external force using force sensor located at the holder of the connection mechanism at the base. This instrument can greatly reduce the cost, and the connection mechanism between the shaft and the base is one of the most convenient and ingenious way of docking the instrument to a robot. But the performance of the instrument is limited because it doesn't has as many degrees of freedom as other designs.

2.2.3 The Advantages of Underactuated Multi-Joint Flexible Robot

Among all the innovations in robotic instruments, multi-joint flexible robot, also known as wire-driven flexible mechanism (WFM), is a kind of robot that has several features that greatly suit SILS applications for its large workspace and underactuated nature which leads to bigger number of flexible joints. Also it uses direct pulling to generate bending moment instead of frictions between tendons and joints. This could be a potential small improvement, because according to DFA data in Alemzadeh et al. (2016a), up to the year of 2013 about 79 of the robotic surgery interruption was caused or resulted in robot instrument failure due to reasons like blood drop caused tendon slipping. And the structure of multi-joint flexible robot dictates that the chance of multi-joint flexible robot tendon slipping

is small enough to be negligible. In Fig. 2.2, the system malfunction is the largest portion among all surgical incidents. This could reflect that tendon slipping is a problem of current instruments even though different measures have been taken to elevates this problem.

In SILS laparoscopic applications, one aspect of the performance is particularly more important. Better triangulation is desired for SILS instruments more than other surgical techniques. We referenced works done by different groups, such as Li et al. (2016a), Li et al. (2016b) and Kato et al. (2016). Their work has provided valid support that the multi-joint flexible robot does has desired workspace for SILS application. Since the robot implementations share similar structure, we take Li et al. (2016a) as an example.

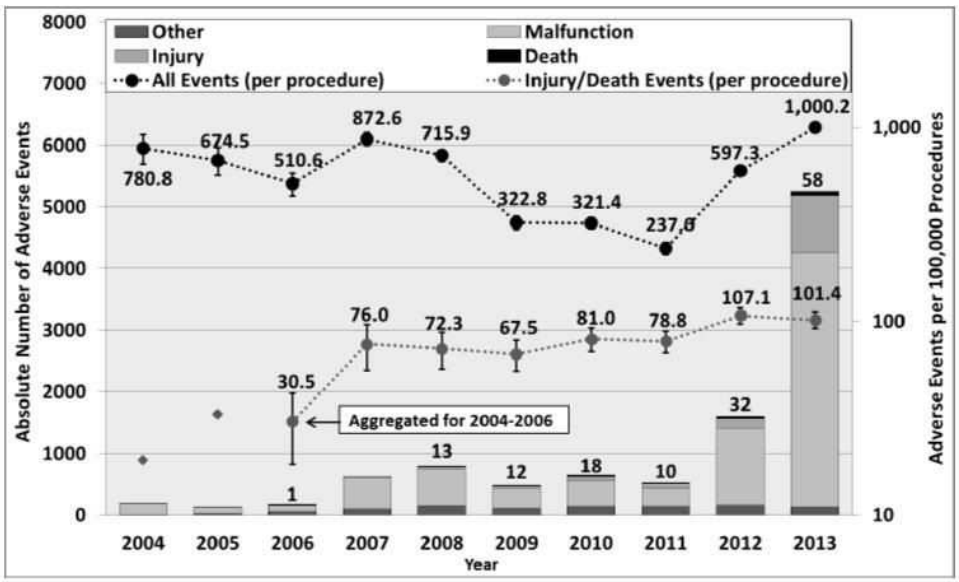

Figure 2.2: FDA Data Reporting Surgery Interruption Alemzadeh et al. (2016b)

Hence we can conclude that multi-joint flexible robot is suitable for developing SILS instruments.

Chapter 3

Design of Surgical Instrument for SILS

We want to design a underactuated multi-joint surgical instrument, up to this point we designed over all structure of the instrument. In order to make up to the low percentage of failures in robotic surgery and control the cost of the system, we picked a manual surgical instrument and designed an actuation pack that will motorize the instrument. So we first study and model the surgical instrument then give the design of actuation pack. We designed an interface that allows it to be integrated with a collaborative robot manipulator, which act as a surgical robot system as an entirety. And without needed to be said, our robotic system is designed toward the flexibility required in SILS and we want to give the system more payload capacity in order to enable the system to do more in surgery by applying parallel mechanism thus reduce the weight.

3.1 Overall Design Plan

The overall design plan is to choose a reliable, flexible and low cost surgical instrument for single incision laparoscopic instrument and design an actuation

pack based on parallel manipulator to construct a robotic surgical instrument and to explore parallel manipulation of underactuated mechanism. The flexible instrument will fundamentally make sure that it is able to conduct surgical, and the actuation pack design will provide motion control and manage to reduce the system weight.

3.2 Surgical Instrument Selection and Its Kinematics

From the first appearance of MIS to the modern advance in robotic technology, there are different designs aim to provide flexibility which vary from each other in terms of structure and material. Structure and material are the two most significant elements that affect the performance of instruments. As we reviewed in the former sections, materials used in the manufacture of laparoscopic instruments can vary from medical purpose stainless steel to medical resin. This exploration in material aims to reduce the weight of the instrument while providing rigidity and flexibility. Without any doubt "perfect" material will make a great instrument but this highly depends on the development of materials science and also this is not one of the essential part of our research.

As we discussed in section 2.2.3, multi-joint flexible robot has its unique features that make it fit in SILS application. Same as other designs like Da Vinci instrument the actuators of multi-joint robot located at the base of the instrument and away from surgical site where surgical liquids mostly appear. And it provides a long flexible part on the instrument wrist which improved triangulation and workspace. It also has a hollow channel in the axial center which allows other major parts like lapoaroscope and different surgical instruments, to be housed. Not only multi-joint flexible robot has common features given above, also there are unique features that suitable for SILS application. multi-joint flexible robot is an underactuated flexible robot which uses pairs of tendon to drive a series of

Figure 3.1: SILS™Manual Instruments

links. This structure makes each link articulatable in two perpendicular directions thus the bendable section of the robot can articulate in two directions unlike other instruments with one DoF on each joint. This increase the flexibility of the instrument wrist and reduced the size of instrument wrist because the one-DoF-on-each instruments has a more complicated structure no matter they are tendon driven or pneumatic driven or other driving method. This greatly limit the total number of DoFs can me implemented on the instrument wrist. However the multi-joint flexible robot ins underactuated robot so it can implement more flexible joints or increase the length of flexible part. Another unique feature of multi-joint flexible robot different from another continuum instrument, the concentric tube robot is that it provides more payload capacity due to the natures of these two mechanisms.

We will study the kinematics and statics analysis of multi-joint flexible robot in order to understand the fundamentals of this mechanism, thus can develop a improved version of actuation pack and push the multi-joint flexible robot further toward SILS application.

3.2.1 Instrument Selection: SILS™by Medtronic

Our design plan is to motorize a well designed surgical instrument suitable for single incision laparoscopic instrument. Our choice is SILS™manual instruments by **Medtronic** shown in Fig. 3.1. SILS instruments have a flexible wrist of tendon-driven underactuated multi-joint flexible mechanism.

Figure 3.2: SILS™Trocar

There are several reasons we chose SILS™by **Medtronic** over other instruments with similar structure. First of all Medtronic is a well-know producer in the medical device business, it has been providing reliable FDA approved medical device for patients over the years. Secondly SILS has the enhanced dexterity on the instrument wrist with a lower price compared to other motorized flexible instrument for single incision laparoscopic surgery but it does not sacrifice the dexterity on the instrument wrist Toshiyuki Mori (2014). Thirdly, SILS™offers a variety of instrument end-effectors including dissect, clinch, shear and hook as shown in Fig. 3.1.

As a single-use surgical instrument it doesn't need to be sterilized, and the cost is fairly low. Each kind of the SILS™instrument has at least 2cm flexible part which allows good triangulation for single incision surgery. And also **Medtronic** provides a well designed trocar as shown in Fig. 3.2 for SILS™.
In our design we picked SILS™Hook as our instrument. It is shown in Fig. 3.3. It has two degree of freedom articulation on the instrument wrist and global positioning which can be provided by an external robot manipulator.

Figure 3.3: SILS™Hook

3.2.2 Kinematics of Multi-joint Flexible Robot

This section is based on work of Li et al. (2015a) as the background knowledge for the design of the actuation mechanism. The system described Li et al. (2015a) has a very similar structure as the kinematic structure as shown in Fig. 3.3. The work is reiterated here for clearance.

Multi-joint robot has underactuated mechanism, it has more flexible joints than actuators. In this case the kinematics refers to the mapping between the displacement of tendons and the end-effector coordinate. The SILS™instrument wrist is controlled by four instrument tendons that are inside the instrument hollow shaft and attached to a plastic knob that is fixed to the ergonomical instrument handle as shown in Fig. 3.3. Therefore articulating the instrument handle controls the instrument wrist. For this section of kinematics modeling 2e are not considering the actuator space which will be discussed in another subsection. We first calculate how the instrument tendon lengths controls the bending angle θ and bending direction ϕ of each flexible joint, Then we calculate task space coordinate with θ and ϕ as shown in Fig. 3.4. From the joint space variables we can derive task space variable, the distal end position x, y and z, bending angle ϑ and bending direction φ. Note that the actuator space means the tendon length change, we will still need to transfer it into actual tendon lengths, but the transformation highly depends on the structure of the actuation setup, we will leave this transformation into actuator space for the next subsection, Mechanical Design. Note that in this section

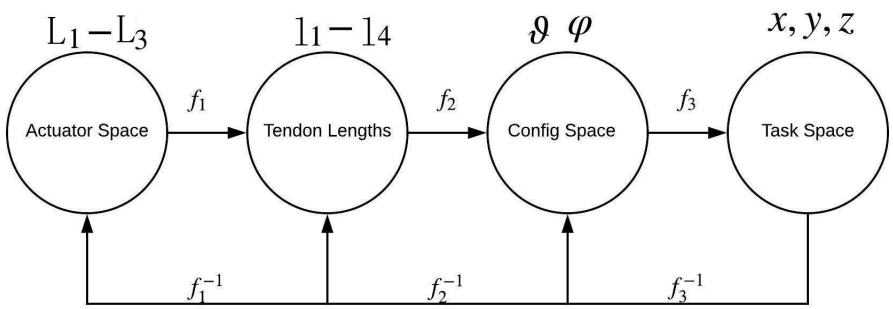

Figure 3.4: Kinematics mappings

we focus on the kinematics of the surgical instrument so the tendons mentioned at the beginning of this subsection means the driving tendons went through the instrument shaft.

Here we use the constant curvature assumption for the flexible wrist of the robot that is the bending angles of each joint on the flexible wrist of the robot are equal to "θ".

We first show the structure of two consecutive flexible or joints of multi-joint flexible robot in Fig. 3.5. Then we consider tendon length change in 2D case. Calculation the tendon on the left and right using supporting lines shown in Fig. 3.6 and Fig. 3.7.

The result of h_r and h_l are:

$$h_r = d - (h_0 \cdot tan\frac{\theta}{2}) \cdot sin\frac{\theta}{2} + \frac{h_0}{cos\frac{\theta}{2}} \tag{3.1}$$

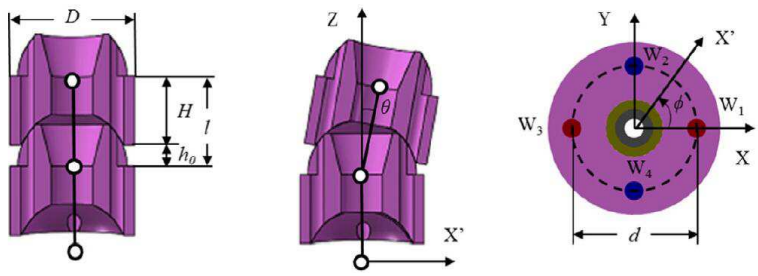

Figure 3.5: Joint Structure and Parameter 3.4

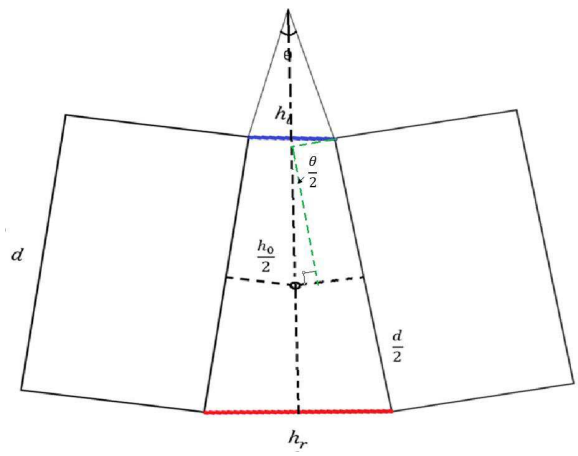

Figure 3.6: Left Tendon Length after Bending

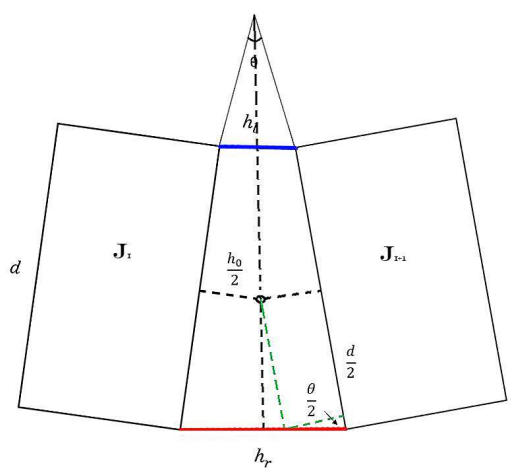

Figure 3.7: Right Tendon Length after Bending

$$h_l = (h_0 - d \cdot tan\frac{\theta}{2}) \cdot cos\frac{\theta}{2} \tag{3.2}$$

Plug in $cos\frac{\theta}{2} = 1 - 2 \cdot sin^2\frac{\theta}{4}$, and we can further simplify the result to:

$$h_r = h_0 + (d \cdot sin\frac{\theta}{2}) - 2h_0 \cdot sin^2\frac{\theta}{4} \tag{3.3}$$

$$h_l = h_0 - (d \cdot sin\frac{\theta}{2}) + 2h_0 \cdot sin^2\frac{\theta}{4} \tag{3.4}$$

Where h_0 is the initial length of tendons when at zero pose. We can tell from these expressions that when bent toward one direction the tendon length changes in one tendon pair are not "symmetric". Combine this result with constant curvature assumption and the total number of flexible joints "N" we can get the total change of tendon length inside instrument shaft in 2D case as:

$$L_r = L_0 + N(h_r - h_0) \tag{3.5}$$

$$L_l = L_0 + N(h_l - h_0) \tag{3.6}$$

If we want to calculate the bending angle ϑ with L_r and L_l:

$$\vartheta = N \cdot 2arcsin\frac{L_r - L_l}{2N_d} \tag{3.7}$$

This only considers 2D case with two tendons, we need to convert this into a two directional bending shown in Fig. 3.8.

Converting from 2 tendons to 4 tendons means change the d parameter which is the distance from the tendons to the center of the instrument. The result is:

$$l_1 = L_0 + N(h_2 - h_0) \tag{3.8}$$

$$l_2 = L_0 + N(h_4 - h_0) \tag{3.9}$$

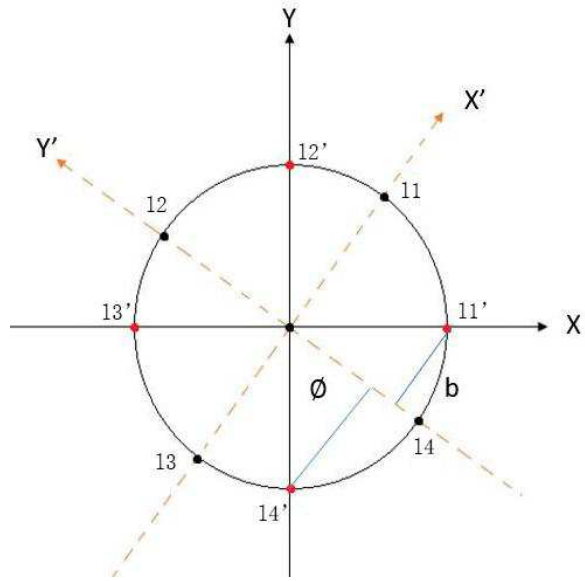

Figure 3.8: Two Directional Bending

$$l_3 = L_0 - N(h_2 + h_0) \tag{3.10}$$

$$l_4 = L_0 - N(h_4 + h_0) \tag{3.11}$$

The same results goes for L_3 and L_4.

$$l_1 = L_0 + N(\frac{d}{2}cos\phi sin\frac{\theta}{2} - h_0 sin^2\frac{\theta}{4}) \tag{3.12}$$

$$l_2 = L_0 + N(\frac{d}{2}sin\phi sin\frac{\theta}{2} - h_0 sin^2\frac{\theta}{4}) \tag{3.13}$$

$$l_3 = L_0 - N(\frac{d}{2}cos\phi sin\frac{\theta}{2} + h_0 sin^2\frac{\theta}{4}) \tag{3.14}$$

$$l_4 = L_0 - N(\frac{d}{2}sin\phi sin\frac{\theta}{2} + h_0 sin^2\frac{\theta}{4}) \tag{3.15}$$

Also we can calculate bending direction ϕ and bending angle θ from L_1 through L_4:

$$\vartheta = 2 \cdot arctan\frac{(l_1 - l_3)^2 + (l_2 - l_4)^2}{2N \cdot d} \tag{3.16}$$

$$\varphi = atan2(l_2 - l_4, l_1 - l_3) \tag{3.17}$$

Those calculation are obtained from equation 3.12 through 3.15, using equation 3.12 minus 3.13 and using equation 3.14 minus 3.15, then we have two equations of variable ϑ and φ. Then we solve for ϑ and φ. As shown in Fig. 3.9, A local frame XYZ is assigned to the center of the first joint. The Z axis is aligned with the robot backbone pointing to the next flexible joint. The angle between the planes XOZ and $X_wO_wZ_w$ is now the bending direction ϕ. Note that the bending direction of each joint equals to the robot bending direction $\phi = \varphi$. The bending angle of each flexible joint is θ and the instrument wrist bending angle $\vartheta = N \cdot \theta$. We already have the joint bending angles θ, we consider in the bending plane XOZ without considering bending direction, the distal end position is:

$$x_t = l \cdot \sum_{N}^{k=1} sin(k \cdot \theta) \tag{3.18}$$

$$z_t = l \cdot \sum_{N}^{k=1} cos(k \cdot \theta) \tag{3.19}$$

Because of the constant curvature assumption, $\vartheta = N \cdot \theta$, the distal position in XZ plane is:

$$x_t = R_f \cdot sin[\vartheta \cdot (N+1)/(2N)] \tag{3.20}$$

$$z_t = R_f \cdot cos[\vartheta \cdot (N+1)/(2N)] \tag{3.21}$$

Where $R_f = \frac{sin(\frac{\theta}{2})}{sin\frac{\theta}{2N_f}}$.

In the $X_wY_wZ_w$, the coordinates of the robot end-effector is obtained by coordinate homogeneous transformation. We first obtain the local frame by translating along the Z axis for the length of the flexible wrist labeled as L_t. Then rotate about the Z axis for ϕ. Thus the transformation matrix is:

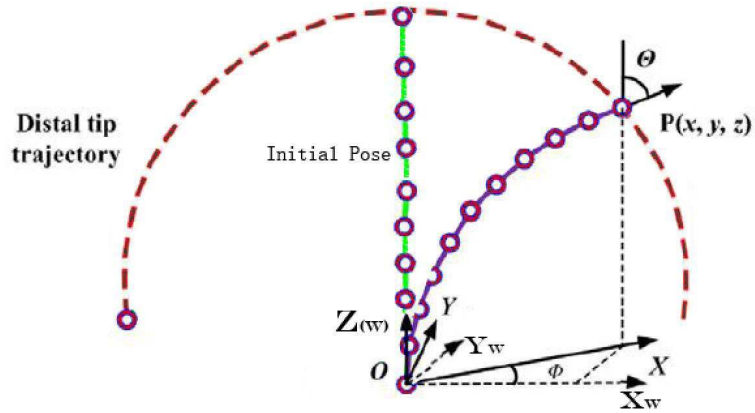

Figure 3.9: Joint Frames Setup Li et al. (2015a)

${}^{w}T_t = {}^{w}T_b \cdot {}^{b}T_t = [Trans_z(x_b)] \cdot [Trans_z(L_t) \cdot Rot_z(\phi)]$ So the end effector pose is:

$$x = x_t \cdot cos(\phi) = R_f sin[\vartheta \cdot (N+1)/(2N)] \cdot cos(\phi) \tag{3.22}$$

$$y = x_t \cdot sin(\phi) = R_f sin[\vartheta \cdot (N+1)/(2N)] \cdot sin(\phi) \tag{3.23}$$

$$z = L_t + z_t = x_t \cdot sin(\phi) = R_f cos[\vartheta \cdot (N+1)/(2N)] \tag{3.24}$$

Now we can say we modeled the kinematics of the underactuated multi-joint flexible robot, one reliable approach to design a surgical instrument with this structure in order to benefit from its enhanced flexibility is to utilize a well design and sealed manual surgical instrument and motorize it. The first advantage of this approach is that we can avoid making any mistake in the instrument design then further avoid surgical risk caused by surgical instrument part, the part that has direct contact with the patient. And secondly, according to FDA data, we know there's a small portion of robotic surgeries went into unexpected mechanical difficulties which caused interruption in surgery, with a detachable surgical instrument installed, surgeon can remove the robotic actuation pack and still have a reliable manual surgical instrument. This might seem not important, but it can shorten the duration of anesthetization and drug dose, and also reduce the

chance of infection because surgeons won't have to retract and re-insert. Thirdly this actuation pack is re-usable and the surgical instrument is well designed and recognized by many hospitals, the cost of the robotic system can be controlled within a reasonable range. For example the surgical instrument in our design is the SILS instrument by **Medtronics**, the cost of this instrument is around 70/Piece while other robotic instruments can easily cost much more. For example, a set of surgical instruments for Da Vinci surgical robot can cost 100000 dollars, given that one set of instruments can be used ten times the instrument cost per surgery can easily be over 10000.

3.3 Mechanical Design of Actuation Pack

In this section we will design a parallel manipulator based actuation pack to control the instrument tendon lengths, thus the end-effector of the underactuated instrument. It is anticipated that we don't have as many DoF as the number of instrument tendons so we will model the actuation pack and the instrument and analyze the results. We will first present the prototype design then give the kinematics modeling of the parallel manipulator. The modeling part consists of inverse and forward kinematics. We will give an initial trajectory and calculate the inverse kinematics to obtain actuation values. The we feed it back to forward kinematics. We want to do this because there is no accurate information for all of the instrument tendons, we can only calculate straight-line distance between points. This is a potential reason for the offset in the calculated results.

We already modeled the kinematics of the underactuated multi-joint flexible robot, so we need to chose a surgical robot with underactuated multi-joint flexible structure and motorize it. SILS Instruments by **Medtronics** came to our sight because it has several advantages. Firstly it has the underactuated multi-joint flexible structure with various instrument end-effector designs including clips, hooks and needles, etc. So with one actuation pack design we can drive different

surgical instrument for all purposes. Secondly it is design and produced by a FDA approved medical device provider so it has been serving in operation rooms since it was introduced to the market. It has proven itself as a reliable surgical tool. And thirdly this instrument has a simple yet effective structure, and a large amount of production which have lead to its reasonable cost. The cost of SILS instruments vary from 50 to 120 depending on the end-effectors. This is certainly desirable because controlling the cost is one of our major goals.

3.3.1 Mechanical Design

According to the structure of SILS instruments, SILS surgical hook in this case, the driving tendons connected to the last joint of the flexible section on the shaft are connected to a cable knob which is constrained to move in a spherical fashion. So the core of our actuation pack is to drive this spherical movement. The cable knob rotates like a universal joint which has two degree of freedom, we will design a structure that drives this "universal joint" without breaking the structure of the instrument in order to enable easy replacement and maintain the rigid structure of the instrument.

The mechanical structure has two tasks, the first is to articulate the tendon plate in two directions, another is to provide housing and support to the instrument. So we designed a tendon plate which the four instrument tendons are attached to, and control the tendon lengths by articulating the tendon plate in a restricted universal articulation.

The structure of our design is shown in Fig. 3.10 Li et al. (2015b). The structure of the actuation is essentially a three degree-of-freedom parallel manipulator whose end-effector or moving platform holds the four instrument tendons. A shaft holder composed of two symmetrical pieces houses the tendon plate and provide fixation to the instrument, therefore relative displacement between instrument shaft and the tendon plate can be generated by changing the lengths of actuator tendons

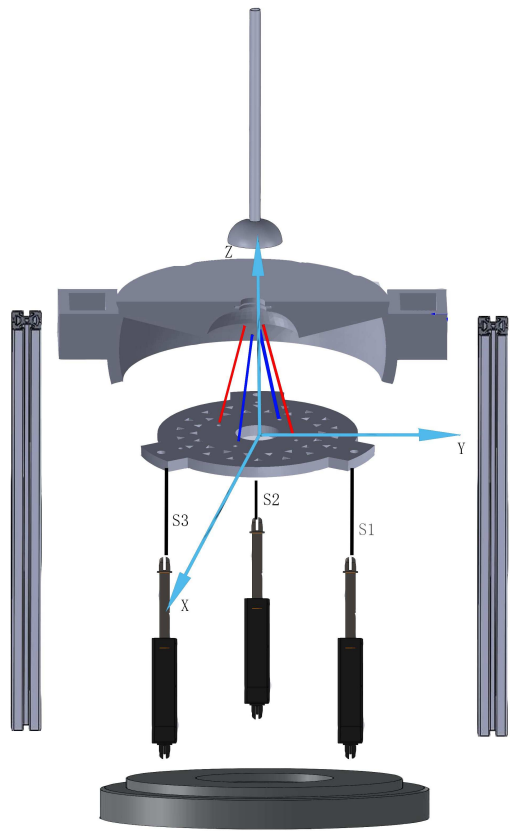

Figure 3.10: Design of Instrument Actuation Pack

which causes the instrument tendons lengths to change thus the articulation of the instrument wrist.

We now calculate the rotation matrix of the tendon plate given articulation angle α and β:

$$T_{plate} = Trotx(\alpha)Troty(\beta)Trans(d) \tag{3.25}$$

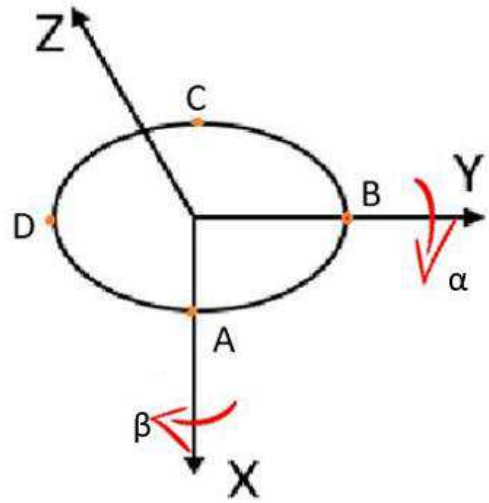

Figure 3.11: Tendon Attachment Points on the Cable Knob

$$= \begin{bmatrix} \cos\beta & 0 & \sin\beta & 0 \\ \sin\alpha\cos\beta & \cos\alpha & -\cos\beta\sin\alpha & 0 \\ -\cos\alpha\sin\beta & \sin\alpha & \cos\alpha\cos\beta & d \\ 0 & 0 & 0 & 1 \end{bmatrix}$$

where $Trotx$ and $Troty$ indicate rotation about x and y axis respectively. And $Trans(0)$ shows there is no translation from the initial frame to the new rotated frame. And we can calculate the vectors $\overrightarrow{SA}$, $\overrightarrow{SB}$, $\overrightarrow{SC}$, and $\overrightarrow{SD}$.

$$\overrightarrow{SA} = \overrightarrow{SO} + T_{plate}^{-1}\overrightarrow{OA} \tag{3.26}$$

$$\overrightarrow{SB} = \overrightarrow{SO} + T_{plate}^{-1}\overrightarrow{OB} \tag{3.27}$$

$$\overrightarrow{SC} = \overrightarrow{SO} + T_{plate}^{-1}\overrightarrow{OC} \tag{3.28}$$

$$\overrightarrow{SD} = \overrightarrow{SO} + T_{plate}^{-1}\overrightarrow{OD} \tag{3.29}$$

Note that in the above calculations, the vectors $\overrightarrow{OA}$, $\overrightarrow{OB}$, $\overrightarrow{OC}$, and $\overrightarrow{OD}$ are in the local rotated frame, we first transform them back to the global from before

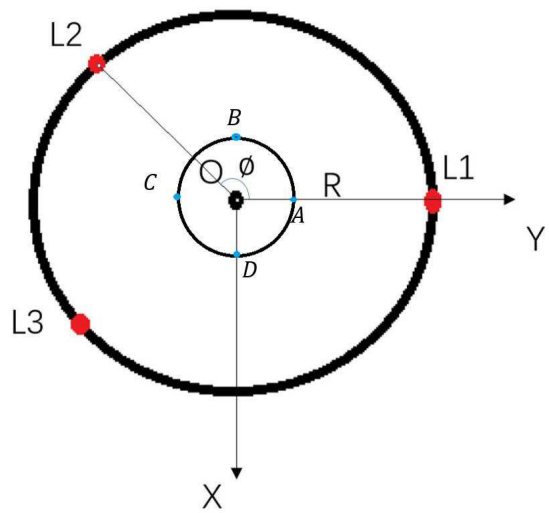

Figure 3.12: Setup of Tendons

we use them to calculate tendon lengths. And the magnitude of $\overrightarrow{SA}$, $\overrightarrow{SB}$, $\overrightarrow{SC}$, and $\overrightarrow{SD}$ shows the tendon length between tendon split point and the attachment points. Considering that the shorter pairs of the tendons affect the articulation of the instrument wrist more, they are the main factors. We can match the value of one or two shortest among $\overrightarrow{SA}$, $\overrightarrow{SB}$, $\overrightarrow{SC}$, and $\overrightarrow{SD}$ and one or two shortest among l_1 through l_4. And then we can calculate the articulation angle α and β with given value(s) of tendon length.

3.3.2 Actuator Space Kinematics Mapping

We use three linear actuators to pull three actuation tendons which are connected to the tendon plate. We now represent the tendon plate as a circle and show the locations of the actuation tendons in Fig. 3.12. L1 L2 L3 are the attachment point of actuation tendons which are actuated by linear actuator 1, 2 and 3. The labeled points, A, B, C and D are the attachment point of the instrument tendons, and the angle between tendons are 120°.

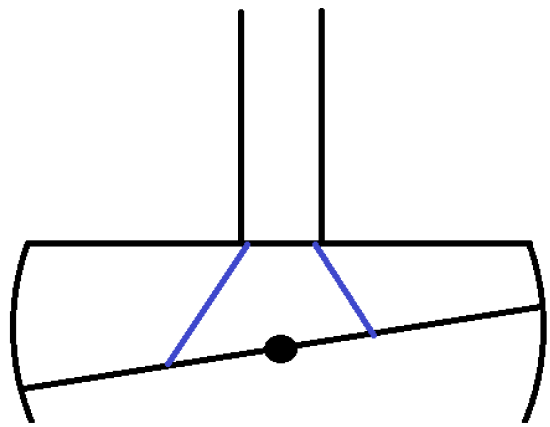

Figure 3.13: Side View of the Tendon Plate Shell

We know the points where four tendons are attached on the cable plate in Fig. 3.11. The points A, B, C and D are the attachment points. We want to calculate the cable length given the lengths of actuator tendons, thus articulation angle θ and ϕ of the tendon plate. In the side view Fig. 3.13, we can see the tendon plate is housed and constrained in the tendon plate shell, the blue lines shows two of the instrument tendons which are a opposite pair.

The zero pose of the tendon plate is shown in Fig. 3.14, the upper circle represents the tendon plate and the lower shows the bottom contour of the tendon plate shell and also the horizontal indicator. After it is articulated an example is exhibited in Fig.3.15. Frame X-Y-Z is the global coordinate frame assigned at the geometrical center of the tendon plate. And X'-Y'-Z' is the frame assigned to the tendon plate body.

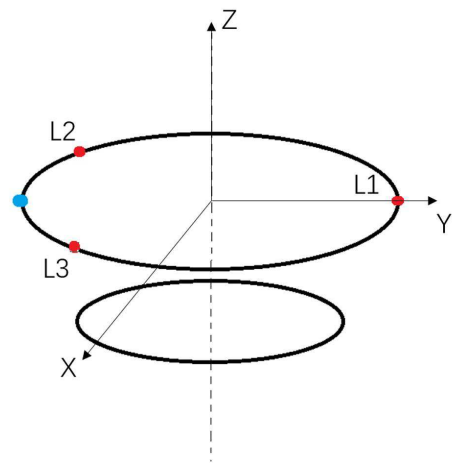

Figure 3.14: Initial position of Tendon Plate

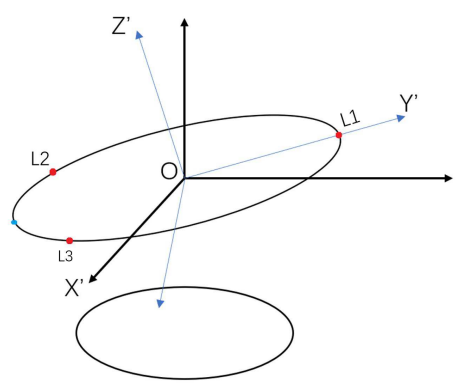

Figure 3.15: Articulated position of Tendon Plate

We now calculate the relationship between actuation tendon lengths and the tendon plate articulation angle α and β. As in Fig.3.16, we can see how the actuation force is conducted from the actuators to the tendon plate. Linear actuators pull the actuator tendons which go through their corresponding channels right above corresponding linear actuator located on the tendon plate shell/shaft holder so that each entry point of actuator tendons into the shaft holder sphere is fixed and can perform linear motion and two degree of freedom rotation. Due to this design, each of the part of the actuator tendons inside the shaft holder sphere can be treated as a Spherical-Prismatic-Spherical(SPS or UPU) leg. That is because the actuator tendons are tightly pulled and backlash and deformation of the tendons

are negligible, and they are actuated by linear actuators and their entry points and connection points to the tendon plates can be treated as two spherical joints with little offset due to the nature of flexible materials. Since the linear actuators are fixed on the actuation base and the entry holes locate right above the center of linear actuators, so all the actuators remain upright. It is worth noticing that the part of the actuation mechanism housed by the shaft shell can be treated as a 3 DoF SPS(or UPU) parallel manipulator. Typical parallel manipulators consist of a fixed base and a end-effector, in this case the tendon plate is the moving platform, the plane determined by three entry points of the actuator tendons is the virtual moving platform. We therefore abstract the 3 DoF parallel manipulator as shown in Fig. 3.17. In Fig. 3.17, we can see B_1 B_2 and B_3 are the actuator tendon entry points who also determines the "base platform" of the parallel manipulator. We name the attachment points of actuator tendons L1, L2 and L3. And the frame O-XYZ is the frame at the moving platform earlier. There is a world frame O'-X'Y'Z' on the fixed base platform.

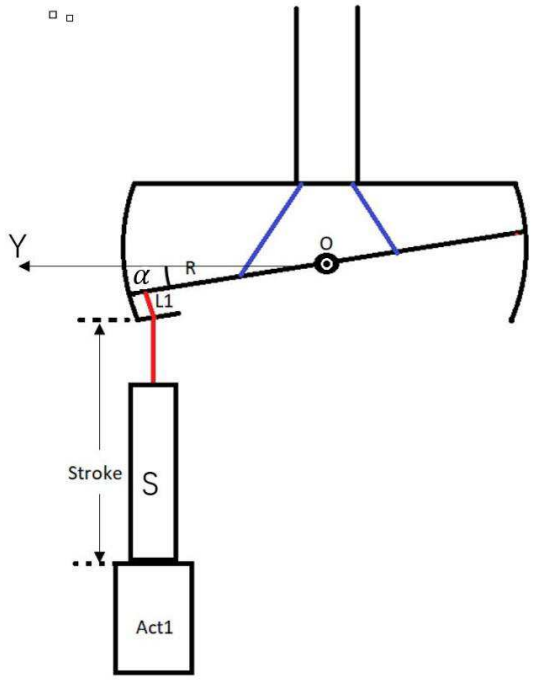

Figure 3.16: Sideview of Actuated Instrument

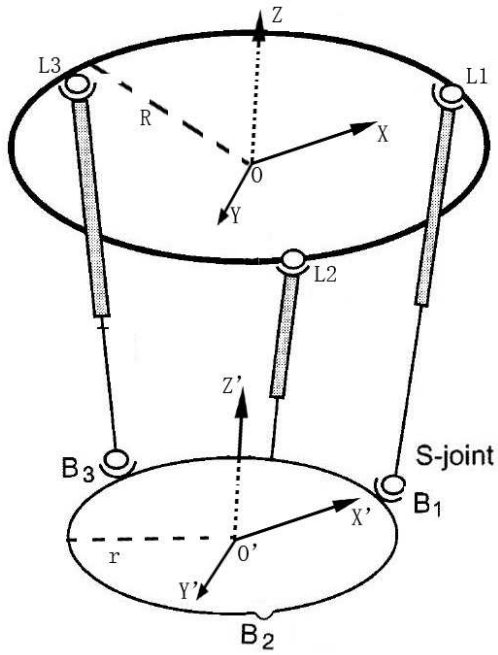

Figure 3.17: Virtual 3 DoF Parallel Manipulator

We set the radius of the $B_1B_2B_3$ plane at $r = 48.21mm$ and the radius of the circle determined by three actuator tendon attachment point at $R = 50mm$. In order to complete the kinematics mapping shown in Fig. 3.4 we need to complete the mapping between actuator space and tendon lengths. This is essentially kinematics problems of parallel manipulators. The tendon lengths can be calculated with the pose of the moving platform of the parallel manipulator Binbin et al. (2011). In this case the calculation of tendon lengths is done in former section. Note that there is a little problem that the instrument tendons which are fixed on a rigid body are under constraints, their lengths vary with the articulation of the moving platform but not independently. Our method is to only match one or two of the tendons which are primary in controlling the pose of the instrument wrist. After the kinematics model, we can show that this method is viable with simulation.

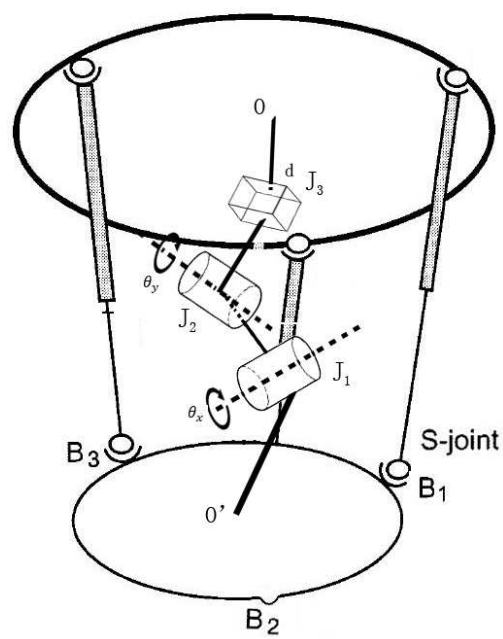

Figure 3.18: Demonstration of Virtual Leg

So for this point the problem has been reduced to calculating the direct and inverse kinematics of a DoF SPS parallel manipulator. We also has a three DoF parallel UPU-legged manipulator with a virtual leg. The virtual serves the purpose of assisting the kinematics modeling. For an actual passive leg the range of motion of the parallel manipulator depending on the configuration of the serial passive leg. But in our case it is a virtual passive leg so there will be no physical restriction on the range of motion of the parallel manipulator Decker et al. (2001), but we still have to chose the parameters carefully so it won't affect the range of motion of the parallel manipulator Decker et al. (2001). Similar problems has been discussed in Joshi and Tsai (2003), Binbin et al. (2011). The inverse kinematics of parallel manipulator calculates the actuator variables given the end-effector poses. Note that in this case even the desired motion of the moving platform is two DoF rotation with out linear translation we still have six task-space variables, $[\theta_x, \theta_y, \theta_z, x, y, z]$, only three of them can be represented independently and we choose these three variables to be $[\theta_x = \alpha, \theta_y = \beta, z]$ and z remains zero. Given the values of α and β we want to calculate the actuator variables, the tendon lengths, vector $\overrightarrow{B_1L1}$, $\overrightarrow{B_2L2}$ and $\overrightarrow{B_3L3}$. Recall that the rotation matrix of the end-effector given three variables are calculated as:

$$T_{plate} = Trotx(\alpha)Troty(\beta)Trans(d) \tag{3.30}$$

$$= \begin{bmatrix} {}^{O}R_{O'} & p \\ 0 & 1 \end{bmatrix}$$

$$= \begin{bmatrix} \cos\beta & 0 & \sin\beta & 0 \\ \sin\alpha\cos\beta & \cos\alpha & -\cos\beta\sin\alpha & 0 \\ -\cos\alpha\sin\beta & \sin\alpha & \cos\alpha\cos\beta & d \\ 0 & 0 & 0 & 1 \end{bmatrix}$$

Where ${}^{O}R_{O'}$ represents rotation and p is the position vector. The actuator tendon vectors are calculated as:

$$\overrightarrow{B_iLi} = T_{plate}\overrightarrow{OLi} + \overrightarrow{O'O} - \overrightarrow{O'B_i} \tag{3.31}$$

This is a simple one step calculation, we will now calculate the forward kinematics of the parallel manipulator.

In the work of Joshi and Tsai (2003), a 4-leg 3 DoF parallel manipulator with 3 actuation robotic legs and one passive leg were proposed. And they calculated kinematics in a closed kinematics chain constructed by the passive leg located at the center of the manipulator. Inspired by their work we add a virtual passive leg to our actuation mechanism in order to construct a closed kinematics chain. The virtual leg is shown in Fig. 3.18, it is a 3 DoF serial manipulator with two revolute joints and one prismatic joint, and the transformation matrix calculated for the virtual passive leg is T_{plate}. And the inverse kinematics of the passive leg is calculated as:

$$\theta_1 = Atan2(\frac{z}{dsin\theta_2}, \frac{y}{dsin\theta_2}) \tag{3.32}$$

$$\theta_2 = cos^{-1}(-\frac{x}{d}) \tag{3.33}$$

$$d = \left|\overrightarrow{OO'}\right| \tag{3.34}$$

Now we choose Euler angles ϑ, ψ and φ to be the task space variables and they can be calculated with θ_1 θ_2 and d:

$$\vartheta = sin^{-1}(-cos\theta_1 sin - \theta_1) \tag{3.35}$$

$$\psi = Atan2(\frac{-cos\theta_1}{cos\theta}, \frac{sin\theta_1 sin\theta_2}{cos\theta}) \tag{3.36}$$

$$\varphi = Atan2(\frac{cos\theta_1 cos\theta_2}{cos\theta}, \frac{sin\theta_2}{cos\theta}) \tag{3.37}$$

In the closed kinematics chain we calculate the tendon lengths:

$$\overrightarrow{B_iLi} = T_{plate}\overrightarrow{OLi} + \overrightarrow{O'O} - \overrightarrow{O'B_i} \tag{3.38}$$

We now label each of the tendon lengths as q_i, and hence:

$$q_i^2 = [T_{plate}\overrightarrow{OLi} + \overrightarrow{O'O} - \overrightarrow{O'B_i}]^T[T_{plate}\overrightarrow{OLi} + \overrightarrow{O'O} - \overrightarrow{O'B_i}] \tag{3.39}$$

we calculate each q_i for $i = 1$, 2 and 3:

$$q_1^2 = d^2 + r^2 + R^2 + Rdcos\theta_2 - 2rRsin\theta_2 \tag{3.40}$$

$$q_2^2 = d^2 + r^2 + R^2 + 2Rdcos^2\beta_3 sin\theta_2 - 2Rdsin\beta_3 cos\theta_1 sin\theta_2 \tag{3.41}$$

$$\begin{aligned} q_3^2 = {} & d^2 + R^2 + r^2 + 2Rdcos\beta_3 cos\theta_2 - 2Rrsin\beta_3 cos\beta_3 cos\theta_1 cos\theta_2 - 2Rrsin^2\beta_3 sin\theta_1 \\ & - 2Rrcos^2\beta_3 sin\theta_2 - 2Rdsin\beta_3 cos\theta_2 sin\theta_2 \end{aligned} \tag{3.42}$$

Where β_2 and β_3 describe the location of $L2/B_2$ and $L3/B_3$, $\beta_2 = 120°$ and $\beta_3 = 240°$.Now we well do some mathematical manipulation to the equations 3.42, we will move q_i and other terms to one side for $i = 1$, 2 and 3.

$$d^2 - 2Rrsin\theta_2 + 2Rdcos\theta_2 + R2^+r^2 - q_1^2 = 0 \tag{3.43}$$

$$\begin{aligned} & d^2 - 2Rrcos\beta_2 sin\beta_2 cos\theta_1 cos\theta_2 - 2Rrcos\beta_2 sin\beta_2 sin\theta_2 - 2Rrcos^2\beta_2 Rrcos^2\beta_2 sin\theta_2 \\ & - 2Rsin\beta_2 cos\theta_1 cos\theta_2 + 2Rcos\beta_2 cos\theta_2 + R^2 + r^2 - q_2^2 = 0 \end{aligned} \tag{3.44}$$

$$d^2 - 2Rrcos\beta_3 sin\beta_3 cos\theta_1 cos\theta_2 - 2R^2 sin^2\beta_3 sin\theta_1 - 2R^2 cos^2\beta_3 sin\theta_2 - 2Rsin\beta_3 cos\theta_1 cos\theta_2$$
$$+ 2Rcos\beta_3 cps\theta_2 + R^2 + r^2 - q_3^2 = 0 \tag{3.45}$$

Now we write those equations as:

$$d^2 + e_{i1} cos\theta_1 cos\theta_2 + e_{i2} sin\theta_1 + e_{i3} sin\theta_2 + e_{i4} dcos\theta_1 sin\theta_2 + e_{i5} dcos\theta_2 + e_{i6} = 0 \tag{3.46}$$

Up to this point we have three equations of d, θ_1, θ_2 and q_i. Now we want to represent two of d, θ_1 and θ_2 with the other one so we can get a high order equation of one variable, thus solving one of d, θ_1, θ_2 solves all three. First we calculate equation 3.43 minus equation 3.44:

$$\begin{aligned}&[(e_{11} - e_{21}) cos\theta_2 + (e_{14} - e_{24} dsin\theta_2)] cos\theta_1 + (e_{12} - e_{22}) sin\theta_1 + d^2 \\ &+ (e_{23} - e_{23}) sin\theta_2 + (e_{15} - e_{25}) dcos\theta_2 = 0\end{aligned} \tag{3.47}$$

And we calculate equation 3.43 minus equation 3.45:

$$\begin{aligned}&[(e_{11} - e_{31}) cos\theta_2 + (e_{12} - e_{32}) dsin\theta_2] cos\theta_1 + (e_{12} - e_{32}) sin\theta_1 + d^2 \\ &+ (e_{13} - e_{33}) sin\theta_2 + (e_{15} - e_{35}) dcos\theta_2 = 0\end{aligned} \tag{3.48}$$

Where e_{ij} are coefficients attached in the Appendix. We now want to eliminate θ_1, so we take equation 3.47 and 3.48 and extract θ_1 and treat the rest as coefficients and obtain:

$$\tilde{e_{11}} cos\theta_1 + \tilde{e_{12}} sin\theta_1 + \tilde{e_{13}} = 0 \tag{3.49}$$

$$\tilde{e_{21}} cos\theta_1 + \tilde{e_{22}} sin\theta_1 + \tilde{e_{23}} = 0 \tag{3.50}$$

Note that $\tilde{e_{ij}}$ are coefficients include $theta_2$ and d. We now have a two variables($\cos\theta_1$ and $\sin\theta_2$) linear equations group, we can solve for $\cos\theta_1$ and $\sin\theta_2$:

$$sin\theta_1 = [e_{\tilde{1}3} - \frac{e_{\tilde{1}1}(e_{\tilde{1}3} - e_{\tilde{2}3})}{e_{\tilde{1}1} - e_{\tilde{2}1}}]\frac{e_{\tilde{1}1} - e_{\tilde{2}1}}{e_{\tilde{1}1}(e_{\tilde{1}2} - e_{\tilde{2}2}) + e_{\tilde{1}2}(e_{\tilde{1}1} - e_{\tilde{2}1})} \tag{3.51}$$

$$cos\theta_1 = (e_{\tilde{2}3} + \frac{e_{\tilde{2}2}e_{\tilde{1}1}}{e_{\tilde{1}2}})\frac{e_{\tilde{1}2}}{e_{\tilde{1}2}(e_{\tilde{1}2} - e_{\tilde{2}2}e_{\tilde{1}1})} \tag{3.52}$$

Since $sin^2\theta_1 + cos^2\theta_1 = 1$ we plug in equation 3.51 and 3.52 and will obtain an equation of θ_2 and d hence θ_1 is eliminated.

$$(e_{\tilde{1}2}e_{\tilde{2}3} - e_{\tilde{1}3}e_{\tilde{2}2})^2 + (e_{\tilde{1}3}e_{\tilde{2}1} - e_{\tilde{1}1}e_{\tilde{2}3})^2 - (e_{\tilde{1}1}e_{\tilde{2}2} - e_{\tilde{1}2}e_{\tilde{2}1})^2 = 0 \tag{3.53}$$

And now we want to eliminate another unknowns among d, θ_1 and θ_2. It is worth noticing that equation 3.41 has no θ_1 term and only d and θ_2 so we can use this equation to eliminate θ_2. We move q_1^2 to the other side of the equation and obtain:

$$d^2 - 2Rr\frac{2tan\frac{\theta_2}{2}}{1 + tan^2\frac{\theta_2}{2}} + 2Rd\frac{1 - tan^2\frac{\theta_2}{2}}{1 + tan^2\frac{\theta_2}{2}} + R^2 + r^2 - q_1^2 = 0 \tag{3.54}$$

And we multiply equation 3.54 by $1 + tan^2\frac{\theta_2}{2}$ and get:

$$(d^2 - 2Rd + R^2 + r^2 - q_1^2)tan^2\frac{\theta_2}{2} - 2Rrtan\frac{\theta_2}{2} + (d^2 + 2Rd - R^2 + r^2 + q_1^2) = 0 \tag{3.55}$$

If we name the coefficients in 3.55 k_{ij} we have one equation:

$$\lambda_{11}tan^2\frac{\theta_2}{2} + \lambda_{12}tan\frac{\theta_2}{2} + \lambda_{13} = 0 \tag{3.56}$$

where λ_{1i} are given in the Appendix. And we now make equation 3.53 a polynomial equation of $tan\frac{\theta_2}{2}$ in the same way.

$$\begin{aligned} &\lambda_{21}tan^8\frac{\theta_2}{2} + \lambda_{22}tan^7\frac{\theta_2}{2} + \lambda_{23}tan^6\frac{\theta_2}{2} \\ &+\lambda_{24}tan^5\frac{\theta_2}{2} + \lambda_{25}tan^4\frac{\theta_2}{2} + \lambda_{26}tan^3\frac{\theta_2}{2} + \\ &\lambda_{27}tan^2\frac{\theta_2}{2} + \lambda_{28}tan^1\frac{\theta_2}{2} + \lambda_{29} = 0 \end{aligned} \tag{3.57}$$

And λ_{2i} are given in the Appendix. Now that we have a polynomial equation of $tan\frac{\theta_2}{2}$ and the coefficients of equation 3.56 and 3.57 contains d, if we can find out an constraint for those coefficients we can calculate d, hence the other two variables. And one common method of calculating kinematics involves high order polynomial equation which can be calculated considering the polynomial equation 3.57 is high order. One solution to this problem is Sylvester's Dialytic Elimination. This method has been used by researchers to eliminate one or two unknowns in kinematics problems. And there are six steps in Dialytic Elimination Raghavan and Roth (1995):

- Rewrite equations with one variable suppressed Raghavan and Roth (1995).
- Define new power products as new homogeneous unknowns Raghavan and Roth (1995).
- Obtain new linear equations so as to has as many linear independent homogeneous equations as linear unknowns Raghavan and Roth (1995).
- Set the coefficient matrix of set of equations formed from former steps to zero and obtain a polynomial in suppressed variable Raghavan and Roth (1995).
- Determine the roots of the polynomial or the eigenvalue of the matrix and yields all the possible values for the suppressed variable Raghavan and Roth (1995).
- Substitute for the suppressed and solve for remaining unknowns Raghavan and Roth (1995).

This is a description of what we've mostly achieved up to this point. Note that we need as as many linear independent homogeneous equations as linear unknowns Raghavan and Roth (1995). So we will multiply equation equation 3.54 by $tan^n\frac{\theta_2}{2}$ for $n = 1$ through $n = 6$ and obtain new set of polynomial equations and multiply

equation 3.55 $tan\frac{\theta_2}{2}$. Hence we have a 10×10 coefficient matrix.

$$\begin{bmatrix} \lambda_{21} & \lambda_{22} & \lambda_{23} & \lambda_{24} & \lambda_{25} & \lambda_{26} & \lambda_{27} & \lambda_{28} & \lambda_{29} & 0 \\ 0 & \lambda_{21} & \lambda_{22} & \lambda_{23} & \lambda_{24} & \lambda_{25} & \lambda_{26} & \lambda_{27} & \lambda_{28} & \lambda_{29} \\ 0 & 0 & 0 & 0 & 0 & 0 & 0 & \lambda_{11} & \lambda_{12} & \lambda_{13} \\ 0 & 0 & 0 & 0 & 0 & 0 & \lambda_{11} & \lambda_{12} & \lambda_{13} & 0 \\ 0 & 0 & 0 & 0 & 0 & \lambda_{11} & \lambda_{12} & \lambda_{13} & 0 & 0 \\ 0 & 0 & 0 & 0 & \lambda_{11} & \lambda_{12} & \lambda_{13} & 0 & 0 & 0 \\ 0 & 0 & 0 & \lambda_{11} & \lambda_{12} & \lambda_{13} & 0 & 0 & 0 & 0 \\ 0 & 0 & \lambda_{11} & \lambda_{12} & \lambda_{13} & 0 & 0 & 0 & 0 & 0 \\ 0 & \lambda_{11} & \lambda_{12} & \lambda_{13} & 0 & 0 & 0 & 0 & 0 & 0 \\ \lambda_{11} & \lambda_{12} & \lambda_{13} & 0 & 0 & 0 & 0 & 0 & 0 & 0 \end{bmatrix}$$

And

$$\sigma = [tan^9\frac{\theta_2}{2}, tan^8\frac{\theta_2}{2}, tan^7\frac{\theta_2}{2}, tan^6\frac{\theta_2}{2}, tan^5\frac{\theta_2}{2}, tan^4\frac{\theta_2}{2}, tan^3\frac{\theta_2}{2}, tan^2\frac{\theta_2}{2}, tan^1\frac{\theta_2}{2}, tan^0\frac{\theta_2}{2}]^T$$

And we now follow the steps in Sylvester's method and set the coefficient matrix to zero. Because he compatibility condition for nontrivial solutions to exist is that the determinant to be zero Joshi and Tsai (2003). And the roots of the new polynomial and the eigenvalue of the matrix will give us all the other variables Raghavan and Roth (1995). And now the forward kinematics problem of the parallel manipulator is solved. We need to associate this to the configuration space. Since the tendon plate introduces constraints to the instrument tendons, we cannot control every instrument tendon at their desired length. But our actuation mechanism is capable of controlling the motion. The idea is to control the one or two main tendons that are being pulled. That is, match the tendon lengths that are being pulled with an appropriate end-effector pose of the parallel manipulator

and ignore the other tendons. Now we prove that our simplification work properly in terms of motion controlling.

Chapter 4

Actuation Pack Hardware Design

In this chapter we will present the hardware design of the actuation mechanism. We will state the structure and dive into different parts.

4.1 Overall Structure

As we stated in former chapters, the surgical instrument design is based on underactuated multi-joint flexible robot and a parallel manipulator. And the core idea of our actuation pack is to maintain the relative position of the instrument shaft and the base of the parallel manipulator and create displacements between instrument shaft and tendon plate hence manipulates the $l1$ through $l4$. So our hardware design serves the following purposes: Provide support and stablization to the surgical instrument, constrain the motion of the tendon plate and actuator tendons, provide housing for actuators, and maintain the fixation of the base of the actuation pack and instrument shaft during actuation. So the assembly of the instrument as shown in Fig. 4.1. It is consisted of instrument, shaft holder shell, tendon plate, actuators, driving tendons, actuator base and external supports.

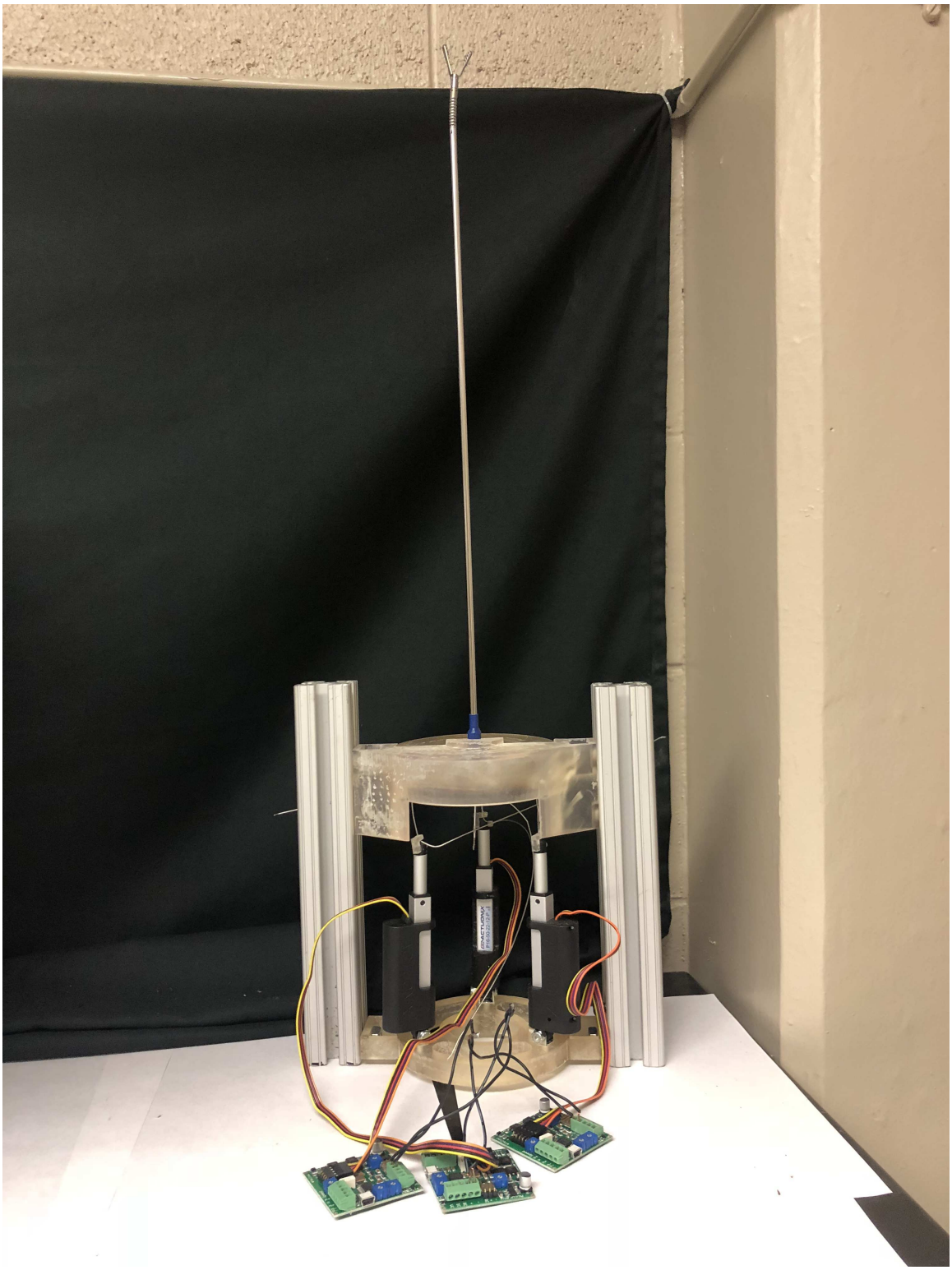

Figure 4.1: Instrument Assembly

4.2 Mechanical Design Annotation

In this section we separately present each part of the actuation pack including their designs and functions.

4.2.1 Flexible Instrument Shaft

The flexible instrument shaft is the end-effector, it houses the instrument tendons and flexible joints of the underactuated flexible instrument wrist. We selected the mechanical design of SILS™because it is a underactuated multi-joint mechanism, and more importantly it is already well packaged for medical purposes. That is to say we don't have to worry about problems neither like the compatibility of the design of the instrument with surgical trocar and other instruments, nor the material of the instrument. As long as our actuation pack serves its purpose the performance of the instrument as assured.

The SILS™has a 5mm diameter hollow shaft which houses two pairs of instrument tendons. The flexible wrist is located at the distal end of the hollow shaft which has nine flexible joints which have a complex mechanical design but follows the rules of flexible joint design: they all have four guide holes for four instrument tendons, and they are designed to perform two DoF universal articulation with respect to the former joint. Hence it can be perfectly classified as a underactuated multi-joint flexible robot. The body length(H) is $1mm$, and the initial gap(h_0) is $1mm$, and the radius of the "instrument tendon circle" is $2mm$. Due to the parameters of the flexible joints and lack of constraint in the mechanical design, the flexible wrist can articulate in a very large range with manual manipulation but most of it is the effect of excessive force but not according to the principle. So we only want to achieve well controlled with a maximum bending angle of 60 degree.

4.2.2 Shaft Holder/ Tendon Plate Shell

One piece of the CAD design of the shaft holder is shown in Fig. 4.2. The shaft holder serves two purposes, providing fixation and constrain the motion of tendon plate. The shaft holder consists of two pieces. They are two mirrored pieces except that one side comes with the interface to the external support. Since the instrument is articulated by rotating tendon plate, it is essential to fix the instrument shaft. We created a tight fit interface on the shaft holder which the complex instrument shaft base is stuck into. Once the piece with interface to the external support is connected to the support, the instrument shaft is fixed to the base of the instrument, hence the relative displacement of tendon plate and the instrument shaft can be realized. Since the tendon plate only performs two DoF rotation without translation, the main body of the shaft holder is a partial sphere. This is because we want to isolate the motion of tendon plate from outside environment to avoid possible collision, and we designed three holes on the lower bottom of shaft holder so that the entry points of three actuation tendons in to the sphere constructed by the shaft holder shell are fixed, which is convenient for modeling because we can thus regard the tendons inside the shaft holder sphere as the legs of the parallel manipulator without considering the actual actuators. Those two pieces of the shaft holder share same instrument shaft interface as shown in Fig. 4.2.

4.2.3 Tendon Plate

The role of the tendon plate in the actuation is essential. It is the connection between instrument wrist and the actuators, and it's also the top platform of the parallel manipulator. So we want the tendon plate to be rigid and able to provide fixation for the seven tendons attached to its body. As shown in Fig. 4.3 and 4.4 the

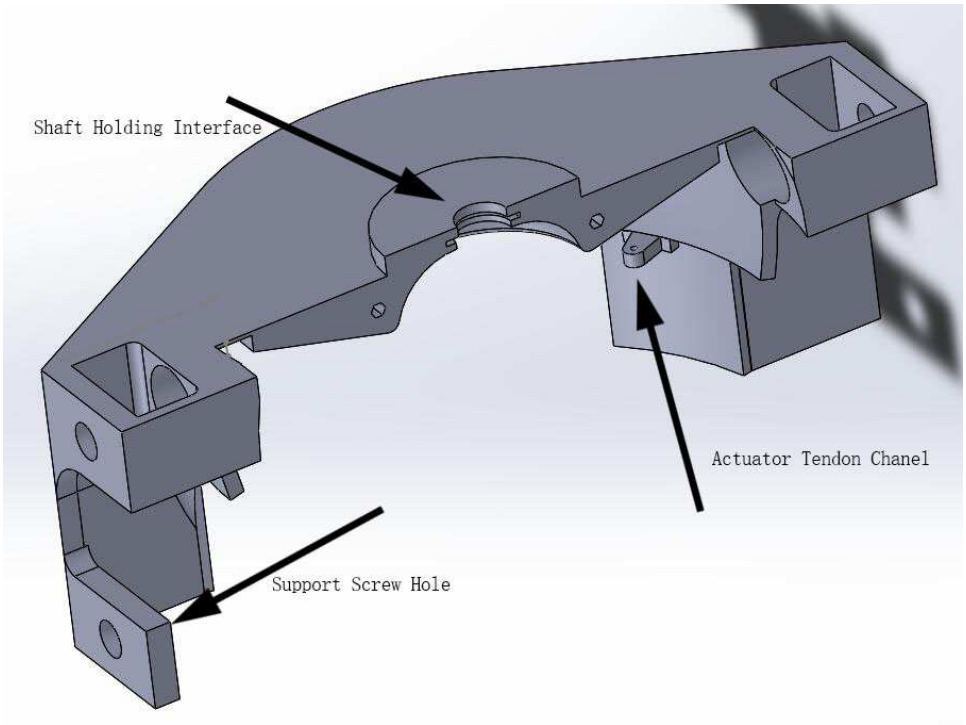

Figure 4.2: Shaft Holder Design with External Support Interface

tendon plate include the plate main body and some supporting pieces for tendon fixation. There two virtual circles, the instrument tendons circle and the actuator tendons circle which mean the circles constructed by the attachment points of corresponding tendons. The radius of the instrument tendon circle is $1cm$ and the radius of the actuator tendon circle is $5cm$. We noticed that the radius of the actuator tendon circle is much larger that is because in order to control the instrument wrist in the desired range we need at approximately $20N$ according to our experiment. To reduce the load on actuators to allows smaller actuator we increased the arm of each actuation force by increasing the radius of the actuator circle.

Another challenge is to provide reliable fixation to the tendons. This can be tricky because the tendon plate is made of resin and the tendons are made of

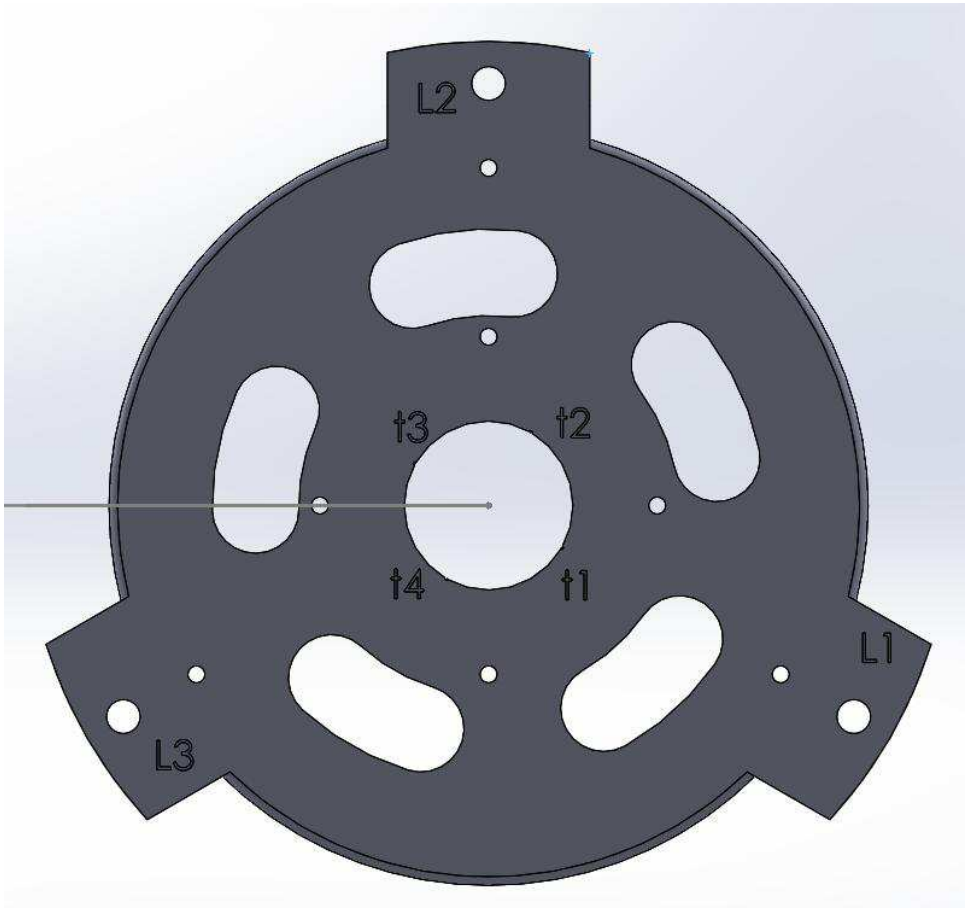

Figure 4.3: Tendon Plate Main Body

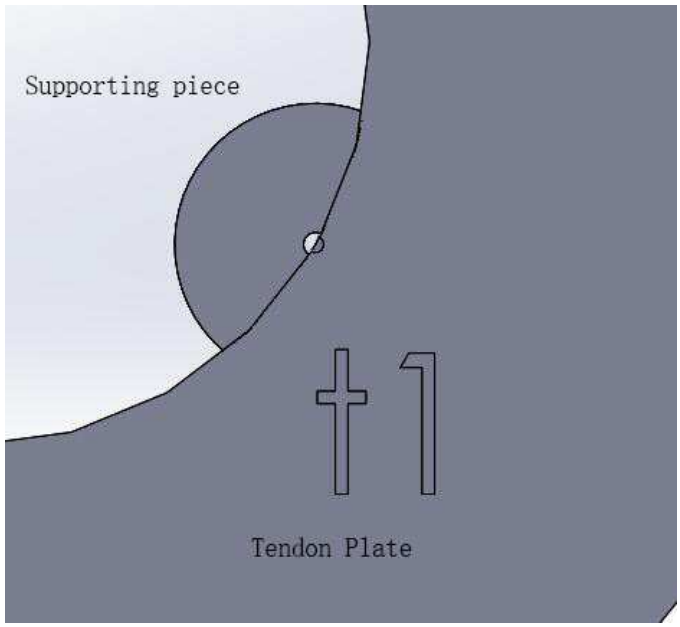

Figure 4.4: Supporting Pieces Installation

alloy, those materials are hard to be glued together. Another approach is to use welding techniques to modify the tendon ends to enable rigid fixation but this was hard under lab condition because it would involve aluminum welding. So the supporting pieces are designed. The end of the instrument tendons has a bulge, so we designed a resin piece that can be glued to the tendon plate. Those two pieces together can fix the tendon on both axial and radial directions.

The actuator tendons don't have bulges so the mechanism we used on instrument tendons will not work here. We designed a catheter circular cylinder with a hollow center which has just the same radius of the tendon. Also it has some holes on the side used to inject super glue into the hollow center in order to provide firm fixation to the tendons.

4.2.4 Base and External Support

The function of the base and external support are simple, supporting the actuation pack. The base supports three actuators, and the external support are connected

to both the base and the shaft holder, so that the actuators can now operate the tendon plate to create change in instrument tendon lengths. We used two T-Slot aluminum rails as external supports because it allows various parts installation points which aids the assembly and easier pre-tension for the tendons.

And as shown in Fig.4.5, the motor base has three mounting points for three motors and still has enough space for other extra potential motors and controllers. The installation of the motor base is similar to the installation of the shaft holder, it is also screwed onto the external support. And all up to this point the mechanical design of each component of the actuation pack is complete.

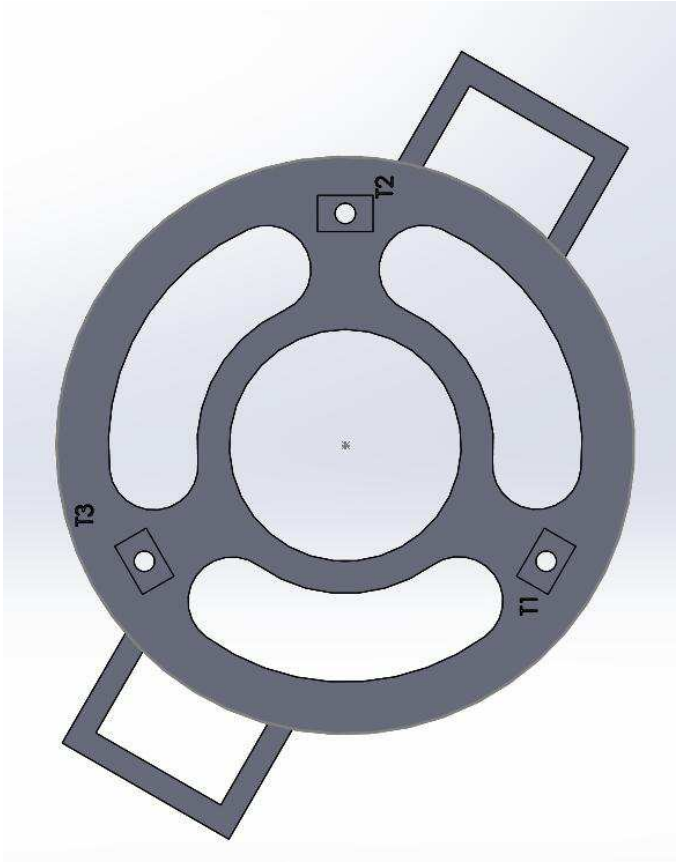

Figure 4.5: Motor Base CAD Design

Chapter 5

Results and Simulation

In this chapter we want to present the result of our design and verify our design performance through simulation.

5.1 Instrument Assembly

The instrument assembly is shown in Fig. 4.1. At this stage we assembled the instrument, including the mechanism that holds the surgical instrument, tendon fixation and parallel manipulator following our design plan. The surgical instrument is locked in place, the tendon plate provides reliable fixation to the instrument tendons and actuator tendons. The tendon plate is contained inside an isolated space so its operation won't affect or get affected. And the actuators are located on the base, along with the part we designed for the actuator tip, the 3 DoF parallel manipulator is constructed.

5.2 Simulation and Analysis

The idea of our simulation is to analyze the potential errors introduced by reduced number of actuators and our mechanical design. Out method is to calculate the variables such as instrument tendon lengths and actuator tendon lengths given a

trajectory, then feed those back to forward kinematics. Through this process we will be able to see how is the performance of the design.

The most ideal design for cable driven robots should provide sufficient degree of actuation in order to fully control the cable driving mechanism. But due to some considerations such as weight control, thermal control and cost management for some designs with large amount of driving cables, underactuated mechanism are proposed, just like our work. It can control more degree of freedom with less actuators. And we want to explore the possibility of using parallel manipulator to control such underactuated mechanism. Because compare to serial manipulator parallel manipulator offers more rigidity and we were able to reduce the weight of the actuation pack. In this section we will discuss our mechanism's ability to fully control the motion of the surgical instrument wristwe. In our design we have four instrument tendons and three actuators. And the actuators along with the tendon plate constructs a three DoF manipulator with UPU legs. And the end-effector affects the lengths of four instrument tendons. Since the tendons are binded together by the tendon plate we want to explore the capability of parallel manipulator in terms of controlling instrument tendon lengths. We perform this assessment following the approach in Fig. 3.4. Given a series of bending angles and we calculate the desired tendon lengths, thus we match the longer instrument tendon lengths without pulling the other two shorter tendons and solve for the linear actuators' desired actuation length. Then we can feed the calculated stroke percentage to forward kinematics model for instrument tendon lengths or the distance between tendon attachment point to tendon separation point.

Choosing a given trajectory is important. Because even though our design is a prototype aiming to explore the kinematics of parallel manipulator control, it is still a surgical robot. So we choose a half circle as the given trajectory because it is the most performed motion in suturing since most suture tasks are performed with "C-shape" suturing needle kit as shown in Fig. 5.1. Not that our input is end-effector bending angle and bending direction because the tasks space coordinates

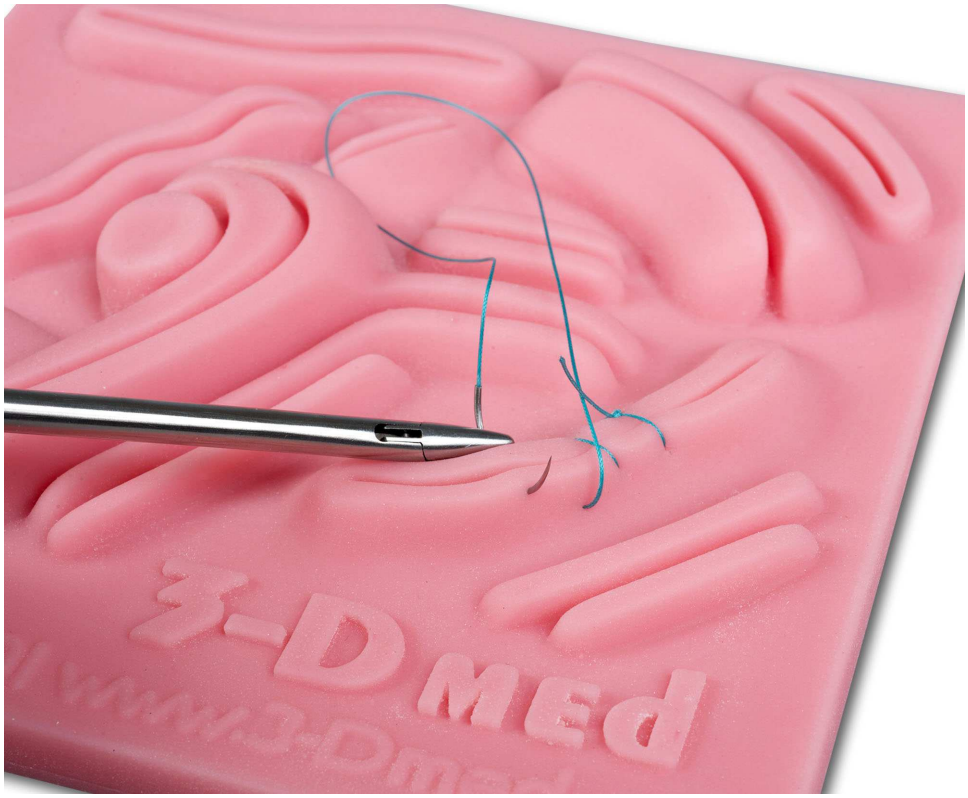

Figure 5.1: Suturing with C-shape Needle

cannot be arbitrary within its range of motion since it highly depend on the placement of surgical robot and positioning is controlled by external operator and instrument actuation. But if we choose bending angle and bending direction as our input it will only be controlled by our actuation mechanism.

Now we show the given trajectory. Since our input isn't task space coordinates, to better visualize the trajectory we plotted sine and cosine of bending direction φ given a bending angle of $\frac{\pi}{4}$ as shown in Fig. 5.2. We put both caltulated trajectory and given trajectory in this figure upfront to show that the simulation result. This is a visualization of the trajectory with given bending angle and bending direction. We can see that there is a small varying difference between the two. It ranges from 0 to $1mm$. It is a small bias. We will analyze the reason later.

Given this half circle we want to calculate the desired instrument tendon lengths,

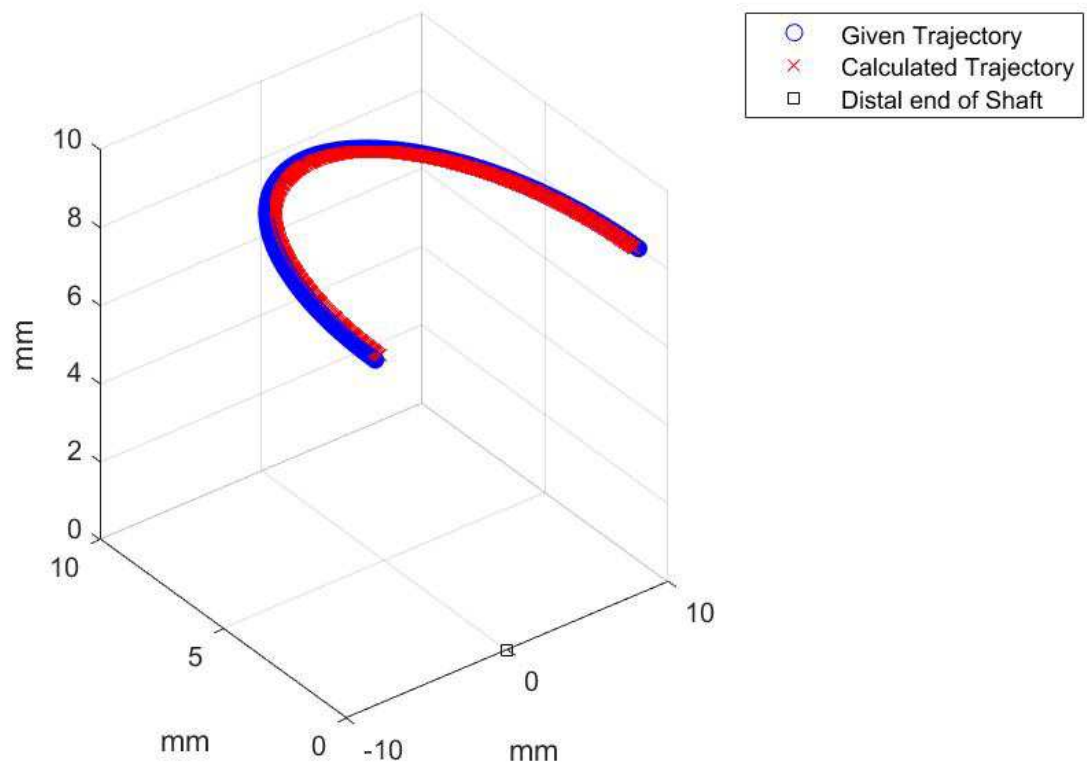

Figure 5.2: Trajectory Comparison between Given Trajectory and Calculated Trajectory

The Blue line shows the given trajectory and the red shows the calculated trajectory. The result has a error of from 0 to 1 mm or 0 to 0.03 rad.

the results are shown in Fig. 5.2. The top row shows the inverse and forward calculation of tendon 1 and 2, while the second row is the results of the inverse and forward calculation of tendon 3 and 4. There are differences between the two results because the forward calculation is not the actual tendon lengths but the distance between instrument attachment lengths and split point. With this method we have no way to obtain the accurate instrument tendon lengths without independent actuator for each tendon. And our design only has two degree of freedom to control four tendons. And we will proceed to calculating the actuation lengths. If we count the number of degree of freedom in instrument shaft we will see that it is also a two DoF mechanism. In this case the two DoF we have in our mechanical design should be enough to control the instrument but we can see that in our simulations it failed. This is the biggest issue of this design approach, we don't have accurate instrument tendon lengths for forward kinematics design which caused the bias in the results in Fig. 5.2. Corresponding instrument tendon lengths match the inverse kinematics calculation while they are pulled at corresponding bending direction. And those errors directly resulted in the errors in the task space coordinates. And we show the results in Fig. 5.4. Three actuation values are shown by three lines in Fig. 5.4. In our results negative values indicates retraction and positive values indicates elongation. There is a small fault in the middle at $\phi = \frac{\pi}{2}$ because at that point the instrument tendons that are pulled just switched to their opposite tendons.

Then we can feed the actuation values to the forward kinematics model and solve for the distances between instrument tendon attachment points and the tendon separation point. The results are shown in Fig. 5.3. And we also monitored the tendon plate articulation angles in Fig. 5.5 The results don't quite match the desired values. This is can be interpreted as the results of the restriction introduced by the tendon plate. As we know the tendon plate is the end-effector of the parallel manipulator. This design reduces the control degree of freedom and since we controlled the parallel manipulator to only perform 2

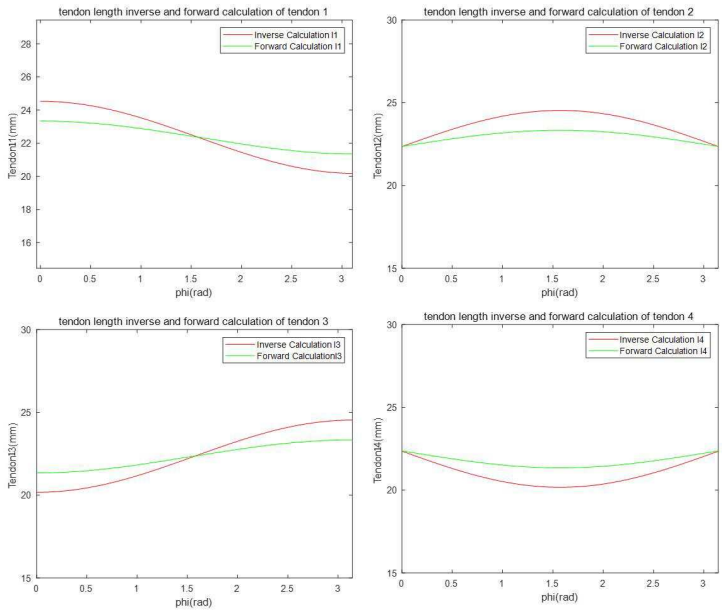

Figure 5.3: Inverse and Forward Instrument Tendon Lengths

The top row shows the calculated instrument tendon 1 and 2 lengths, while the bottom row shows the calculated instrument tendon 3 and 4 lengths in our forward kinematics.

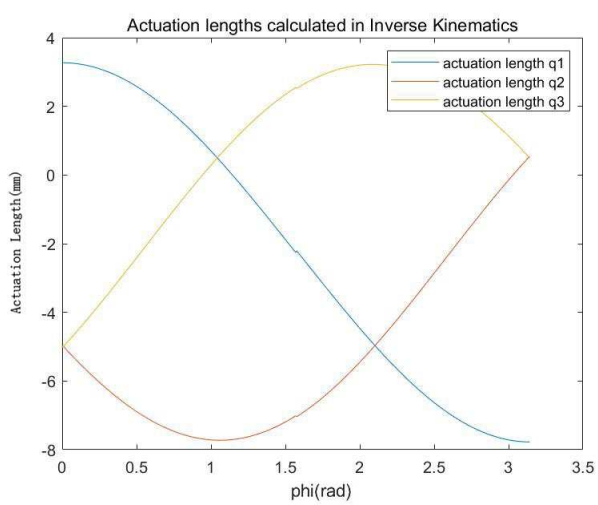

Figure 5.4: Actuation Lengths

DoF rotation, the control degree of freedom is further reduced. The results has proven the restriction, there are sudden change in tendon plate articulation angles because at certain bending direction the tendon lengths we matched changed. One possible approach is to remove the tendon plate shell which contains the tendon plate's motion, that allows us to release the full degree of freedom of the parallel manipulator. From equation 3.12 through 3.17, we can calculate the bending direction and bending angle given perfect control of instrument tendon lengths. But in this case we cannot fully control all lengths, for the most cases we can control two of the tendon lengths and if we try to solve the bending angle and bending direction with two equations from 3.12 through 3.17 we cannot solve the unique solution. So we used the resultant distances as our imaginary tendon lengths to solve for bending angle and bending direction for reference as shown as calculated trajectory in Fig. 5.2. Compared to the given pose as shown in Fig. 5.2, we choose x axis as the bending angles and y axis as the bending directions. Recall our given trajectory is a half-circle with a constant bending angle and varying bending direction from 0 to π, it is shown in Fig. 5.2 at a specific bending angle the bending direction varies from 0 to π. Since our calculated result as shown in the figure there is slight offset in bending angle for around $0.1rad$. This is because of the fact that the tendons that are not under tension are longer than the straight-line distance between tendon attachment point and the tendon split point. As expected there will be offsets, and it is expected. Any visible offset is considered to be unacceptable especially in surgical field.

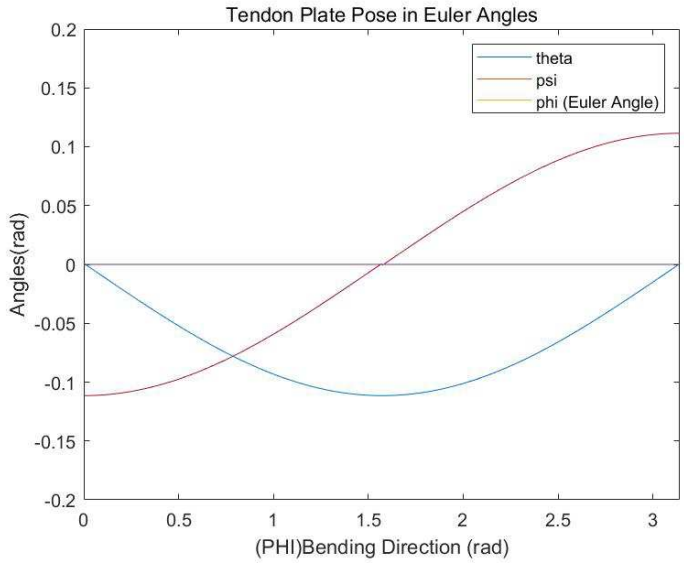

Figure 5.5: Tendon Plate Articulation angles

The inverse and forward kinematics are exactly the same so we only draw one set. The Tendon Plate pose consists of three Euler Angles but the pan motion doesn't exist, so one of them is always zero. And the small fault is because at that certain point the instrument tendons which are pulled switched.

Chapter 6

Conclusion

We've designed the structure and hardware of the robotic instrument and in this part we want to discuss how the simulations reflect the effectiveness of this design. We designed a parallel manipulator based actuation mechanism because this allows us to reduce weight of the actuation mechanism. However, due to the reduced number of actuation degree of freedom there will be some drawbacks. We were unable to obtain the exact lengths of some of the instrument tendons because the instrument tendons are attached to the tendon plate and we don't have actuator for each instrument tendon which lead to the lack of accurate information on instrument tendons lengths that are not under tension. So in forward kinematics calculation we can only obtain some of the straight-line distance between the tendon attachment points to the instrument split point. And due to the reduced number of freedom there can't be accurate control on all the tendon lengths, and their attachment points are fixed on a rigid body tendon plate which is another constraint on the tendon lengths control. In our design there is a partial spherical shaft holder which was designed mainly to contain the tendon plate while it's in motion. Aside from the contained motion which increases safety it also introduced another constraint on the range of motion. It in fact reduced the three DoF motion to two DoF. But to obtain exact lengths of instrument tendons and fully control

all tendons it is desirable to apply separate actuators to each tendon. As a result there is offset in the calculated result for as much as $0.03Rad$. So according to our simulation this design did reduce the number of actuators, but it comes with the sacrifice in control. We don't have accurate information on all the instrument tendon lengths and we cannot control each instrument tendons separately because we reduced the number of actuators to reduce the system weight. There are errors between given trajectory and calculated trajectory in simulation results, so we can conclude that this design is not ideal for controlling precision robots like surgical robots. But still it was a meaningful process of exploring the possibility of parallel manipulator based control. Underactuated multi-joint robot has many features that are suitable for application in confined space. It possesses more flexibility but only requires fewer actuators which reduces size, weight of the system. Through this project we can explore the underactuated control to control the joints on the distal end with fewer actuators located remotely.

The idea of the "3-DoF parallel manipulator" became an option because parallel manipulator offers more rigidity and stability considering its size and power, and me personally have interests in studying some kinematics of parallel manipulators. We wanted one single mechanical part to provide fixation to four instrument tendons, and parallel manipulators can provide more stability and actuation force with the same size actuators as serial manipulators. I considered this project as a chance, so the parallel manipulator based actuation mechanism was designed. We designed each part of the system and assembled the system. The assembling process has followed the design plan. And we tried to verify the functionality and explored the performance of the actuation mechanism. In the most common move in suturing process, the simulation results has showed that due to the effect of the tendon plate and reduced number of degree of freedom the tendon length control cannot be performed accurately. But it is a inevitable for any underactuated mechanism. Parallel mechanism we designed cannot fully control every DoF. In our case the instrument tendons aren't tensed by actuators all the time, but it gave

me the chance to study parallel mechanism and underactuated robots.

Our idea of designing a parallel based actuation pack was based on the desire of reducing system weight so some sacrifice of performance was made. In the end we verified he limitation this design approach has. Our design did reduce the number of actuators applied thus reduced the system weight. But the reduced number of actuators cannot give us enough information on all instrument tendons lengths and cannot fully control all instrument tendons. Compactness is important in surgical fields because surgical robot has limited payload capacity, it is always desirable for the development of more compact surgical instruments because the more compact instrument itself is, the more the surgical robotic system can offer to aid the surgeons. At the same time, surgical applications are one of the few fields with the highest demand on precision. Safety is the top priority, so when we design surgical robots we want to find the perfect balance point between compactness and precision. This design was a exploration on one of the possible approaches of finding the balance point, and the result indicates that more advanced and delicate design for single-incision laparoscopic surgery need to be optimized for better surgical outcomes.

Bibliography

A. Seneci, C., Leibrandt, K., Wisanuvej, P., Shang, J., Darzi, A., and Yang, G.-Z. (2016). Design of a smart 3d-printed wristed robotic surgical instrument with embedded force sensing and modularity. 11, 12, 14

Alemzadeh, H., Raman, J., Leveson, N., Kalbarczyk, Z., and Iyer, R. K. (2016a). Adverse events in robotic surgery: A retrospective study of 14 years of fda data. *PLOS ONE*, 11(4):1–20. 14

Alemzadeh, H., Raman, J., Leveson, N., Kalbarczyk, Z., and Iyer, R. K. (2016b). Adverse events in robotic surgery: A retrospective study of 14 years of fda data. *PLoS One*, 11(4):e0151470–e0151470. 27097160[pmid]. 15

Binbin, P., Zengming, L., Kai, W., and Yu, S. (2011). Kinematic characteristics of 3-upu parallel manipulator in singularity and its application. *International Journal of Advanced Robotic Systems*, 8(4):34. 36, 37

Decker, M. W., Dang, A. X., and Ebert-Uphoff, I. (2001). Motion planning for active acceleration compensation. In *Proceedings 2001 ICRA. IEEE International Conference on Robotics and Automation (Cat. No.01CH37164)*, volume 2, pages 1257–1264 vol.2. 37

Hannaford, B., Rosen, J., Friedman, D. W., King, H., Roan, P., Cheng, L., Glozman, D., Ma, J., Kosari, S. N., and White, L. (2013). Raven-II: an open platform for surgical robotics research. *IEEE Trans Biomed Eng*, 60(4):954–959. 11, 13

Haraguchi, D., Kanno, T., Tadano, K., and Kawashima, K. (2015). A pneumatically driven surgical manipulator with a flexible distal joint capable of force sensing. *IEEE/ASME Transactions on Mechatronics*, 20(6):2950–2961. 13

Jelínek, F., Pessers, R., and Breedveld, P. (2014). Dragonflex smart steerable laparoscopic instrument. *Journal of Medical Devices*, 8(1):015001–015001–9. 9

Joshi, S. A. and Tsai, L.-W. (2003). The kinematics of a class of 3-dof, 4-legged parallel manipulators. *Journal of Mechanical Design*, 125(1):52–60. 37, 38, 43

Kato, T., Okumura, I., Kose, H., Takagi, K., and Hata, N. (2016). Tendon-driven continuum robot for neuroendoscopy: validation of extended kinematic mapping for hysteresis operation. *International Journal of Computer Assisted Radiology and Surgery*, 11(4):589–602. 15

Lee, D. H., Kim, U., Gulrez, T., Yoon, W. J., Hannaford, B., and Choi, H. R. (2016). A laparoscopic grasping tool with force sensing capability. *IEEE/ASME Transactions on Mechatronics*, 21(1):130–141. 12

Lee, S.-J., Lee, S.-C., and Ahn, H.-S. (2014). Design and control of tele-matched surgery robot. *Mechatronics*, 24(5):395 – 406. 11, 13

Leonard, S., Wu, K. L., Kim, Y., Krieger, A., and Kim, P. C. W. (2014). Smart tissue anastomosis robot (star): A vision-guided robotics system for laparoscopic suturing. *IEEE Transactions on Biomedical Engineering*, 61(4):1305–1317. 10

Li, Z., Ren, H., Chiu, P. W. Y., Du, R., and Yu, H. (2016a). A novel constrained wire-driven flexible mechanism and its kinematic analysis. *Mechanism and Machine Theory*, 95:59 – 75. 15

Li, Z., Ren, H., Chiu, P. W. Y., Du, R., and Yu, H. (2016b). A novel constrained wire-driven flexible mechanism and its kinematic analysis. *Mechanism and Machine Theory*, 95:59 – 75. 15

Li, Z., Yu, H., Ren, H., Chiu, P., and Du, R. (2015a). A novel constrained tendon-driven serpentine manipulator. pages 5966–5971. 20, 26

Li, Z., Zin Oo, M., Nalam, V., Duc Thang, V., Yu, H., Ren, H., and Kofidis, T. (2015b). Design of a novel flexible endoscope-cardioscope. page V05BT08A001. 28

Lum, M. J. H., Friedman, D. C. W., Sankaranarayanan, G., King, H., Fodero, K., Leuschke, R., Hannaford, B., Rosen, J., and Sinanan, M. N. (2009). The raven: Design and validation of a telesurgery system. *The International Journal of Robotics Research*, 28(9):1183–1197. 11

Piccigallo, M., Scarfogliero, U., Quaglia, C., Petroni, G., Valdastri, P., Menciassi, A., and Dario, P. (2010). Design of a novel bimanual robotic system for single-port laparoscopy. *IEEE/ASME Transactions on Mechatronics*, 15(6):871–878. 12

Pourghodrat, A., Nelson, C. A., and Oleynikov, D. (2017). Hydraulic robotic surgical tool changing manipulator. *J Med Device*, 11(1):0110081–110086. 28450979[pmid]. 6

Raghavan, M. and Roth, B. (1995). Solving polynomial systems for the kinematic analysis and synthesis of mechanisms and robot manipulators. *Journal of Mechanical Design*, 117(B):71–79. 42, 43

Shang, J., Leibrandt, K., Giataganas, P., Vitiello, V., Seneci, C. A., Wisanuvej, P., Liu, J., Gras, G., Clark, J., Darzi, A., and Yang, G. Z. (2017). A single-port robotic system for transanal microsurgery x2014;design and validation. *IEEE Robotics and Automation Letters*, 2(3):1510–1517. 12

Silva, A. J., Ramirez, O. A. D., Vega, V. P., and Oliver, J. P. O. (2009). Phantom omni haptic device: Kinematic and manipulability. In *2009 Electronics, Robotics and Automotive Mechanics Conference (CERMA)*, pages 193–198. 11

Tan, A., Ashrafian, H., Scott, A. J., Mason, S. E., Harling, L., Athanasiou, T., and Darzi, A. (2016). Robotic surgery: disruptive innovation or unfulfilled promise? a systematic review and meta-analysis of the first 30years. *Surgical Endoscopy*, 30(10):4330–4352. 10

Toshiyuki Mori, Professor of Surgery, K. U. (2014). *Reduced Port Laparoscopic Surgery*. 19

Appendix

Appendix A

Summary of Equations

A.1 Cartesian

$e_{11} = 0$

$e_{12} = 0$

$e_{13} = -2Rr$

$e_{14} = 0$

$e_{15} = 2R$

$e_{16} = R^2 + r^2 - q_1^2$

$e_{21} = -2Rrcos\beta_2 sin\beta_2$

$e_{22} = -2Rrsin^2\beta_2$

$e_{23} = -2Rrcos^2\beta_2$

$e_{24} = -2Rsin^2\beta_2$

$e_{25} = -2Rcos^2\beta_2$

$e_{25} = -2Rcos^2\beta_2$

$e_{26} = R^2 + r^2 - q_2^2$

$e_{31} = -2Rrcos\beta_3 sin\beta_3$

$e_{32} = -2Rrsin^2\beta_3$

$e_{33} = -2Rrcos^2\beta_3$

$e_{34} = -2Rsin^2\beta_3$

$e_{35} = -2Rcos^2\beta_3$

$e_{35} = -2Rcos^2\beta_3$

$e_{36} = R^2 + r^2 - q_3^2$

$\tilde{e_{11}} = (e_{11} - e_{21})cos\theta_2 + (e_{14} - e_{24})dsin\theta_2$

$\tilde{e_{12}} = e_{12} - e_{22}$

$\tilde{e_{13}} = (d^2 + e_{13} - e_{23})cos\theta_2 + (e_{15} - e_{25})dcos\theta_2$

$\tilde{e_{21}} = (e_{11} - e_{31})cos\theta_2 + (e_{14} - e_{34})dsin\theta_2$

$\tilde{e_{22}} = e_{12} - e_{32}$

$\tilde{e_{23}} = (d^2 + e_{13} - e_{33})cos\theta_2 + (e_{15} - e_{35})dcos\theta_2$

$\lambda_{11} = d^2 + 2Rd + R^2 + r^2$

$\lambda_{12} = 2Rr$

$\lambda_{13} = d^2 + 2Rd - R^2 - r^2 + q_1^2$

$\lambda_{21} = d^2(e_{15}-e_{25})^2+(e_{12}-e_{22})^2+d^2(e_{11}-e_{21})^2(e_{16}-e_{36})^2-2d^2(e_{12}-e_{22})(e_{15}-e_{25})(e_{12}-e_{32})(e_{16}-e_{36})-2d^2(e_{11}-e_{21})(e_{15}-e_{25})(e_{11}-e_{21})(e_{16}-e_{36})-2d(e_{15}-e_{25})(e_{16}-e_{26})(e_{12}-e_{32})^2+2d(e_{11}-e_{21})(e_{16}-e_{26})(e_{11}-e_{21})(e_{16}-e_{36})+2d(e_{12}-e_{22})(e_{15}-e_{25})(e_{12}-e_{32})(e_{16}-e_{36})-2d(e_{15}-e_{25})(e_{16}-e_{26})(e_{11}-e_{32})^2+2d(e_{11}-e_{21})(e_{15}-e_{25})(e_{11}-e_{31})(e_{16}-e_{36})+2d(e_{12}-e_{32})(e_{15}-e_{25})(e_{12}-e_{32})(e_{16}-e_{36})-2d(e_{11}-e_{21})^2(e_{16}-e_{36})^2-2d(e_{12}-e_{22})^2(e_{16}-e_{36})^2-(e_{12}-e_{22})^2(e_{11}-e_{31})^2+(e_{11}-e_{31})^2(e_{16}-e_{36})^2+(e_{12}-e_{22})^2(e_{16}-e_{36})^2-2(e_{11}-e_{21})(e_{16}-e_{26})(e_{11}-e_{31})(e_{16}-e_{36})+(e_{16}-e_{26})^2(e_{11}-e_{31})^2+(e_{16}-e_{26})^2(e_{11}-e_{31})^2-2(e_{12}-e_{22})(e_{16}-e_{26})(e_{12}-e_{32})(e_{16}-e_{36})+2(e_{11}-e_{21})(e_{12}-e_{22})(e_{11}-e_{31})(e_{12}-e_{32})-(e_{11}-e_{21})^2(e_{12}-e_{32})^2$

$\lambda_{22} = -4d(e_{13}-e_{23})(e_{15}-e_{25})(e_{11}-e_{31})^2+4(e_{13}-e_{23})(e_{16}-e_{26})(e_{11}-e_{31})^2-4d(e_{12}-e_{22})(e_{14}-e_{24})(e_{11}-e_{31})(e_{12}-e_{32})^2+4(e_{13}-e_{23})(e_{16}-e_{26})(e_{12}-e_{32})^2+4d(e_{11}-e_{21})(e_{15}-e_{25})(e_{11}-e_{31})(e_{13}-e_{33})-4(e_{12}-e_{22})(e_{16}-e_{26})(e_{12}-e_{32})(e_{13}-e_{33})+4d(e_{12}-e_{22})^2(e_{11}-e_{31})(e_{14}-e_{34})-4d^3(e_{15}-e_{25})^2(e_{11}-e_{31})(e_{14}-e_{34})+8d^3(e_{15}-e_{25})(e_{16}-e_{26})(e_{11}-e_{31})(e_{14}-e_{34})-4d(e_{11}-e_{31})(e_{16}-e_{36})^2(e_{14}-e_{34})-4d(e_{11}-e_{21})(e_{12}-e_{22})(e_{12}-e_{32})(e_{14}-e_{32})+4d(e_{11}-e_{21})(e_{13}-e_{23})(e_{11}-e_{31})(e_{16}-e_{36})+4d^3(e_{14}-e_{24})(e_{15}-e_{25})(e_{11}-e_{31})(e_{16}-e_{36})-4d^2(e_{14}-e_{24})(e_{16}-e_{26})(e_{11}-e_{31})(e_{16}-e_{36})+4d(e_{12}-e_{22})(e_{13}-e_{23})(e_{12}-e_{32})(e_{16}-e_{36})-$

$4d^2(e_{14}-e_{24})(e_{15}-e_{25})(e_{11}-e_{31})(e_{16}-e_{36})+4d(e_{14}-e_{24})(e_{16}-e_{26})(e_{11}-e_{31})(e_{16}-e_{36})-$
$4(e_{12}-e_{22})(e_{13}-e_{23})(e_{12}-e_{32})(e_{16}-e_{36})+4(e_{11}-e_{21})^2(e_{13}-e_{33})(e_{16}-e_{36})+4(e_{12}-$
$e_{22})^2(e_{13}-e_{33})(e_{16}-e_{36})-4d^2(e_{11}-e_{21})(e_{15}-e_{25})(e_{14}-e_{34})(e_{16}-e_{36})+4d(e_{11}-e_{21})(e_{16}-$
$e_{26})(e_{14}-e_{34})(e_{16}-e_{36})+8d^2(e_{11}-e_{21})(e_{14}-e_{34})(e_{16}-e_{36})-d(e_{11}-e_{21})(e_{14}-e_{24})(e_{16}-e_{36})^2$
$\lambda_{23}=4(e_{13}-e_{23})^2(e_{11}-e_{31})^2-4d^2(e_{15}-e_{25})^2(e_{11}-e_{31})^2+4d(e_{15}-e_{25})(e_{16}-e_{26})(e_{11}-$
$e_{31})^2+4(e_{13}-e_{23})(e_{12}-e_{32})^2-4d^2(e_{14}-e_{24})^2(e_{12}-e_{32})^2-4d(e_{15}-e_{25})(e_{16}-e_{26})(e_{12}-$
$e_{32})^2-4d(e_{15}-e_{25})(e_{16}-e_{26})(e_{12}-e_{32})^2-4(e_{16}-e_{26})^2(e_{12}-e_{32})^2-8(e_{11}-e_{21})(e_{13}-$
$e_{23})(e_{11}-e_{31})(e_{13}-e_{33})-8d^2(e_{14}-e_{24})(e_{15}-e_{25})(e_{11}-e_{31})(e_{13}-e_{33})+8d(e_{14}-e_{24})(e_{16}-$
$e_{26})(e_{11}-e_{21})(e_{11}-e_{31})(e_{13}-e_{33})-8(e_{12}-e_{22})(e_{13}-e_{23})(e_{12}-e_{32})(e_{13}-e_{33})+8(e_{11}-$
$e_{21})^2(e_{13}-e_{33})^2+16d^2(e_{13}-e_{23})(e_{15}-e_{25})(e_{11}-e_{31})(e_{14}-e_{34})-16d(e_{13}-e_{23})(e_{11}-$
$e_{31})(e_{16}-e_{26})(e_{11}-e_{31})(e_{14}-e_{34})+8d^2(e_{11}-e_{21})(e_{12}-e_{32})(e_{14}-e_{34})-8d^2(e_{11}-e_{21})(e_{15}-$
$e_{25})(e_{13}-e_{33})(e_{14}-e_{34})+8d(e_{11}-e_{21})(e_{16}-e_{26})(e_{13}-e_{33})(e_{14}-e_{34})-4d^2(e_{12}-e_{22})^2(e_{14}-$
$e_{34})^2 4d^4(e_{15}-e_{25})^2(e_{14}-e_{24})^2-8d^3(e_{15}-e_{25})(e_{16}-e_{26})(e_{14}-e_{34})^2+4d^2(e_{16}-e_{26})^2(e_{14}-$
$e_{34})^2-8d^2(e_{13}-e_{23})(e_{14}-e_{24})(e_{11}-e_{31})(e_{16}-e_{36})+8d^2(e_{11}-e_{21})(e_{15}-e_{25})(e_{11}-e_{31})(e_{16}-$
$e_{36})-4d(e_{11}-e_{21})(e_{16}-e_{26})(e_{11}-e_{21})(e_{16}-e_{36})+4d(e_{12}-e_{22})(e_{16}-e_{26})(e_{12}-e_{32})(e_{16}-$
$e_{36})+16d^2(e_{11}-e_{21})(e_{14}-e_{24})(e_{13}-e_{33})(e_{16}-e_{36})-8d^2(e_{11}-e_{21})(e_{13}-e_{23})(e_{14}-e_{34})(e_{16}-$
$e_{36})-8d^4(e_{14}-e_{24})(e_{15}-e_{25})(e_{14}-e_{34})(e_{16}-e_{36})+8d^3(e_{14}-e_{24})(e_{16}-e_{26})(e_{14}-e_{34})(e_{16}-$
$e_{36})-4d^2(e_{11}-e_{21})^2(e_{16}-e_{36})^2+4d^4(e_{14}-e_{24})^2(e_{16}-e_{36})^2+8d(e_{13}-e_{23})(e_{14}-e_{24})(e_{11}-$
$e_{31})(e_{16}-e_{36})-4d(e_{11}-e_{21})(e_{15}-e_{25})(e_{11}-e_{31})(e_{16}-e_{36})+4d(e_{12}-e_{22})(e_{15}-e_{25})(e_{12}-$
$e_{32})(e_{16}-e_{36})-8(e_{12}-e_{22})(e_{16}-e_{26})(e_{12}-e_{32})(e_{16}-e_{36})-16(e_{13}-e_{33})(e_{16}-e_{36})+$
$8d(e_{11}-e_{21})(e_{13}-e_{23})(e_{14}-e_{34})(e_{16}-e_{36})+8d^3(e_{14}-e_{24})(e_{15}-e_{25})(e_{14}-e_{34})(e_{16}-$
$e_{36})-8d^2(e_{14}-e_{24})(e_{16}-e_{26})(e_{14}-e_{34})(e_{16}-e_{36})+4d(e_{11}-e_{21})^2(e_{16}-e_{26})(e_{16}-e_{36})-$
$4d(e_{12}-e_{22})^2(e_{16}-e_{26})(e_{16}-e_{36})-8d^3(e_{14}-e_{24})^2(e_{16}-e_{36})^2+4d(e_{12}-e_{22})^2(e_{16}-e_{36})^2+$
$4d^2(e_{14}-e_{34})^2(e_{16}-e_{36})^2$
$\lambda_{24}=12d(e_{13}-e_{23})(e_{15}-e_{25})(e_{11}-e_{31})^2-4(e_{13}-e_{23})(e_{16}-e_{26})(e_{11}-e_{31})^2-4d(e_{12}-$
$e_{22})(e_{14}-e_{24})(e_{11}-e_{31})(e_{12}-e_{32})+4d(e_{11}-e_{21})(e_{14}-e_{24})(e_{12}-e_{32})^2-4d(e_{13}-e_{23})(e_{15}-$
$e_{25})(e_{12}-e_{32})^2+12(e_{13}-e_{23})(e_{16}-e_{26})(e_{12}-e_{32})^2+16d(e_{13}-e_{23})(e_{14}-e_{24})(e_{11}-e_{31})(e_{13}-$
$e_{33})-12d(e_{11}-e_{21})(e_{15}-e_{25})(e_{11}-e_{31})(e_{13}-e_{33})+4(e_{11}-e_{21})(e_{16}-e_{26})(e_{11}-e_{31})(e_{13}-$
$e_{33})+4d(e_{12}-e_{22})(e_{15}-e_{25})(e_{12}-e_{32})(e_{13}-e_{33})-12(e_{12}-e_{22})(e_{16}-e_{26})(e_{12}-e_{32})(e_{13}-$

$e_{33})-16d(e_{11}-e_{21})(e_{14}-e_{24})(e_{13}-e_{33})^2+4d(e_{12}-e_{22})^2(e_{11}-e_{31})(e_{14}-e_{34})-16d(e_{13}-e_{23})^2(e_{11}-e_{31})(e_{14}-e_{34})+12d^3(e_{11}-e_{31})(e_{14}-e_{34})+12d^3(e_{15}-e_{25})^2(e_{11}-e_{31})(e_{14}-e_{34})-8^2(e_{15}-e_{25})(e_{16}-e_{26})(e_{11}-e_{31})(e_{14}-e_{34})-4d(e_{16}-e_{26})^2(e_{11}-e_{31})(e_{14}-e_{34})-4d(e_{11}-e_{21})(e_{12}-e_{22})(e_{12}-e_{32})(e_{14}-e_{34})+16d(e_{11}-e_{21})(e_{13}-e_{23})(e_{13}-e_{33})(e_{14}-e_{34})+16d^3(e_{14}-e_{24})(e_{15}-e_{25})(e_{13}-e_{33})(e_{14}-e_{34})-16d^2(e_{14}-e_{24})(e_{16}-e_{26})(e_{13}-e_{33})(e_{14}-e_{34})-16d^3(e_{13}-e_{23})(e_{15}-e_{25})(e_{14}-e_{34})^2+16d^2(e_{13}-e_{23})(e_{16}-e_{26})(e_{14}-e_{34})^2-12d(e_{11}-e_{21})(e_{11}-e_{31})(e_{16}-e_{36})-12d^3(e_{14}-e_{24})(e_{15}-e_{25})(e_{11}-e_{31})(e_{16}-e_{36})+4d^2(e_{14}-e_{24})(e_{16}-e_{26})(e_{11}-e_{21})(e_{16}-e_{36})+4d(e_{12}-e_{22})(e_{13}-e_{23})(e_{12}-e_{32})(e_{16}-e_{36})+12d(e_{11}-e_{21})^2(e_{13}-e_{33})(e_{16}-e_{36})-4d(e_{12}-e_{22})^2(e_{13}-e_{33})(e_{16}-e_{36})-16d^3(e_{14}-e_{24})^2(e_{13}-e_{33})(e_{16}-e_{36})+16d^3(e_{13}-e_{23})(e_{14}-e_{24})(e_{14}-e_{34})(e_{16}-e_{36})+12d^3(e_{11}-e_{21})(e_{15}-e_{25})(e_{14}-e_{34})(e_{16}-e_{36})+4d^2(e_{11}-e_{21})(e_{16}-e_{26})(e_{14}-e_{34})(e_{16}-e_{36})+12d^3(e_{11}-e_{21})(e_{14}-e_{24})(e_{16}-e_{36})^2+4(e_{11}-e_{21})(e_{13}-e_{23})(e_{11}-e_{31})(e_{16}-e_{36})+4d^2(e_{14}-e_{24})(e_{15}-e_{25})(e_{11}-e_{31})(e_{16}-e_{36})+4d(e_{14}-e_{24})(e_{16}-e_{26})(e_{11}-e_{31})(e_{16}-e_{36})-12(e_{12}-e_{22})(e_{13}-e_{23})(e_{12}-e_{32})(e_{16}-e_{36})-4(e_{11}-e_{21})^2(e_{13}-e_{33})(e_{16}-e_{36})+12(e_{12}-e_{22})^2(e_{13}-e_{33})(e_{16}-e_{36})+16d^2(e_{14}-e_{24})^2(e_{13}-e_{33})(e_{16}-e_{36})-16d^2(e_{13}-e_{23})(e_{14}-e_{24})(e_{14}-e_{34})(e_{16}-e_{26})+4d^2(e_{11}-e_{21})(e_{15}-e_{25})(e_{14}-e_{34})(e_{16}-e_{36})+4d(e_{11}-e_{21})(e_{16}-e_{26})(e_{14}-e_{34})(e_{16}-e_{36})-8d^2(e_{11}-e_{21})(e_{14}-e_{24})(e_{16}-e_{26})(e_{16}-e_{36})-4d(e_{11}-e_{21})(e_{14}-e_{24})(e_{16}-e_{36})^2$

$\lambda_{25}=2(e_{12}-e_{22})^2(e_{11}-e_{31})^2-8(e_{13}-e_{23})^2(e_{11}-e_{31})^2+6d^2(e_{15}-e_{25})(e_{11}-e_{31})^2-2(e_{16}-e_{26})^2(e_{11}-e_{31})^2-4(e_{11}-e_{21})(e_{12}-e_{22})(e_{11}-e_{31})(e_{12}-e_{32})+2(e_{11}-e_{21})^2(e_{12}-e_{32})^2+8(e_{13}-e_{32})^2-8d^2(e_{14}-e_{24})^2(e_{12}-e_{32})^2-2d^2(e_{15}-e_{25})^2(e_{12}-e_{32})^2+6(e_{16}-e_{26})^2(e_{12}-e_{32})^2+16(e_{11}-e_{21})(e_{13}-e_{23})(e_{11}-e_{31})(e_{13}-e_{33})+16d^2(e_{14}-e_{24})(e_{15}-e_{25})(e_{11}-e_{31})(e_{13}-e_{33})-16d^2(e_{12}-e_{22})(e_{13}-e_{23})(e_{12}-e_{32})(e_{13}-e_{33})-8(e_{11}-e_{21})^2(e_{13}-e_{33})+16d^2(e_{14}-e_{24})^2(e_{13}-e_{33})^2-32d^2(e_{13}-e_{23})(e_{15}-e_{25})(e_{11}-e_{31})(e_{14}-e_{34})+16d^2(e_{12}-e_{22})(e_{14}-e_{24})(e_{12}-e_{32})(e_{14}-e_{34})-32d^2(e_{13}-e_{23})(e_{14}-e_{24})(e_{13}-e_{33})(e_{14}-e_{34})+16(e_{11}-e_{21})(e_{15}-e_{25})(e_{13}-e_{33})(e_{14}-e_{34})-8d^2(e_{12}-e_{22})^2(e_{14}-e_{34})^2+16d^2(e_{13}-e_{23})^2(e_{14}-e_{34})^2-8d^4(e_{15}-e_{25})^2(e_{14}-e_{34})^2+8d^2(e_{16}-e_{26})^2(e_{14}-e_{34})^2+16d^2(e_{13}-e_{23})(e_{14}-e_{24})(e_{11}-e_{31})(e_{16}-e_{26})-12d^2(e_{11}-e_{21})(e_{15}-e_{25})(e_{11}-e_{31})(e_{16}-e_{36})-32d^2(e_{11}-e_{21})(e_{14}-e_{24})(e_{13}-e_{33})(e_{16}-e_{36})+16d^2(e_{11}-e_{21})(e_{13}-e_{23})(e_{14}-e_{34})(e_{16}-e_{36})+16d^4(e_{14}-e_{24})(e_{15}-e_{25})(e_{14}-e_{34})(e_{16}-e_{36})+6d^2(e_{11}-e_{21})^2(e_{16}-e_{36})^2(e_{14}-e_{34})(e_{16}-e_{36})^2+2d^2(e_{12}-e_{22})^2(e_{16}-$

$e_{36})^2 - 8d^4(e_{14}-e_{24})^2(e_{16}-e_{36}) - 12(e_{12}-e_{22})(e_{16}-e_{26}) - 16d^2(e_{14}-e_{24})(e_{16}-e_{26})(e_{14}-$
$e_{34})(e_{16}-e_{26}) - 2(e_{11}-e_{21})^2 + 6(e_{12}-e_{22})^2(e_{16}-e_{26})^2 + 8d^2(e_{16}-e_{36})^2$
$\lambda_{27} = 4(e_{13}-e_{23})^2(e_{11}-e_{31})^2 - 4d(e_{15}-e_{25})^2(e_{11}-e_{31})^2 - 4d(e_{15}-e_{25})(e_{16}-e_{26})(e_{11}-$
$e_{31})^2 + 4(e_{13}-e_{23})^2(e_{12}-e_{32})^2 - 4d^2(e_{14}-e_{24})^2(e_{13}-e_{32})^2 + 4d(e_{15}-e_{25})(e_{16}-e_{26})(e_{12}-$
$e_{32})^2 + 4(e_{16}-e_{26})^2(e_{12}-e_{32})^2 - 8(e_{11}-e_{21})(e_{13}-e_{23})(e_{11}-e_{31})(e_{13}-e_{33}) - 8d^2(e_{14}-$
$e_{24})(e_{15}-e_{25})(e_{11}-e_{31})(e_{13}-e_{33}) - 8d(e_{14}-e_{24})(e_{16}-e_{26})(e_{11}-e_{31})(e_{13}-e_{33}) - 8(e_{12}-$
$e_{22})(e_{13}-e_{23})(e_{12}-e_{32}) + 4(e_{12}-e_{22})^2 + (e_{13}-e_{33}) + 16d^2(e_{13}-e_{23})(e_{15}-e_{25})(e_{11}-e_{31})(e_{14}-$
$e_{34}) + 16(e_{13}-e_{23})d(e_{16}-e_{26})(e_{11}-e_{31})(e_{14}-e_{34}) + 8d^2(e_{12}-e_{22})(e_{14}-e_{24})(e_{12}-e_{32})(e_{14}-$
$e_{34}) - 8d^2(e_{11}-e_{21})(e_{15}-e_{25})(e_{13}-e_{33})(e_{14}-e_{34}) - 4d^2(e_{12}-e_{22})^2(e_{14}-e_{34})^2 + 4d^4(e_{15}-$
$e_{25})^2(e_{14}-e_{34})^2 + 8d^3(e_{15}-e_{25})(e_{16}-e_{26})(e_{14}-e_{34})^2 + 4d^2(e_{16}-e_{26})^2(e_{14}-e_{34})^2 + 8d^4(e_{13}-$
$e_{23})(e_{14}-e_{24})(e_{11}-e_{31})(e_{16}-e_{36}) + 8d^2(e_{11}-e_{21})(e_{15}-e_{25})(e_{11}-e_{31})(e_{16}-e_{36}) + 4d(e_{11}-$
$e_{21})(e_{16}-e_{26})(e_{11}-e_{31})(e_{16}-e_{36}) - 4d(e_{12}-e_{22})(e_{16}-e_{26})(e_{12}-e_{32})(e_{16}-e_{36}) + 16d^2(e_{11}-$
$e_{21})(e_{14}-e_{24})(e_{13}-e_{33})(e_{16}-e_{36}) - 8d^2(e_{11}-e_{21})(e_{13}-e_{23})(e_{14}-e_{34})(e_{16}-e_{36}) - 8d^4(e_{14}-$
$e_{24})(e_{15}-e_{25})(e_{14}-e_{34})(e_{16}-e_{36}) - 8d^2(e_{14}-e_{24})(e_{16}-e_{26})(e_{14}-e_{34})(e_{16}-e_{36}) - 4d^2(e_{14}-$
$e_{24}) + 4d^4(e_{14}-e_{24})^2(e_{16}-e_{36})^2 - 8d(e_{13}-e_{23})(e_{14}-e_{24})(e_{11}-e_{31})(e_{16}-e_{36}) + 4d(e_{11}-$
$e_{21})(e_{15}-e_{25})(e_{11}-e_{31})(e_{16}-e_{36}) - 4d(e_{12}-e_{22})(e_{15}-e_{25})(e_{12}-e_{32})(e_{16}-e_{36}) - 8(e_{12}-$
$e_{22})(e_{16}-e_{26})(e_{12}-e_{32})(e_{16}-e_{36}) + 16d(e_{11}-e_{21})(e_{14}-e_{24})(e_{13}-e_{33})(e_{16}-e_{36}) - 8d(e_{11}-$
$e_{21})(e_{13}-e_{33})(e_{14}-e_{34})(e_{16}-e_{36}) - 8d(e_{11}-e_{21})(e_{13}-e_{23})(e_{14}-e_{34})(e_{16}-e_{36}) - 8d^3(e_{14}-$
$e_{24})(e_{15}-e_{25})(e_{14}-e_{36})(e_{14}-e_{36}) - 8d^2(e_{14}-e_{24})(e_{16}-e_{26})(e_{14}-e_{34})(e_{16}-e_{36}) - 4d(e_{11}-$
$e_{21})^2(e_{16}-e_{36})^2 + 4d(e_{12}-e_{22})^2(e_{16}-e_{36})^2 + 8d^3(e_{14}-e_{24})^2(e_{16}-e_{36})^2 + 4(e_{12}-e_{22})^2(e_{16}-$
$e_{36})^2 + 4d(e_{14}-e_{24})^2(e_{16}-e_{36})^2$
$\lambda_{28} = 4d(e_{13}-e_{23})(e_{15}-e_{25})(e_{11}-e_{31})^2 + 4(e_{13}-e_{23})(e_{16}-e_{26})(e_{11}-e_{31})^2 + 4d(e_{12}-$
$e_{22})(e_{14}-e_{24})(e_{11}-e_{31})(e_{12}-e_{32}) - 4d(e_{11}-e_{21})(e_{14}-e_{24})(e_{12}-e_{32})^2 + 4d(e_{13}-e_{23})(e_{16}-$
$e_{26})(e_{12}-e_{32})^2 - 4d(e_{12}-e_{22})(e_{15}-e_{25})(e_{11}-e_{31})(e_{13}-e_{33}) - 4(e_{11}-e_{21})(e_{16}-e_{26})(e_{11}-$
$e_{31})(e_{13}-e_{33}) - 4d(e_{12}-e_{22})(e_{15}-e_{25})(e_{12}-e_{22})(e_{13}-e_{33}) - 4(e_{12}-e_{22})(e_{16}-e_{26})(e_{12}-$
$e_{32}) - 4d^2(e_{12}-e_{22})^2(e_{11}-e_{31})(e_{13}-e_{33}) - 4d^2(e_{12}-e_{22})^2(e_{11}-e_{31})(e_{14}-e_{34}) + 4d^3(e_{15}-$
$e_{25})^2(e_{11}-e_{31})(e_{14}-e_{34}) + 8d^2(e_{15}-e_{25})(e_{16}-e_{26})(e_{11}-e_{31})(e_{14}-e_{34}) + 4d(e_{16}-e_{26})^2(e_{11}-$
$e_{31})(e_{14}-e_{34}) + 4d(e_{11}-e_{21})(e_{12}-e_{22})(e_{12}-e_{32})(e_{14}-e_{34}) - 4d(e_{11}-e_{21})(e_{13}-e_{23})(e_{11}-$
$e_{31})(e_{16}-e_{36}) - 4d^3(e_{14}-e_{24})(e_{15}-e_{25})(e_{11}-e_{31})(e_{16}-e_{36}) - 4d^2(e_{14}-e_{24})(e_{16}-e_{26})(e_{11}-$

$e_{31})(e_{16}-e_{36})-4d(e_{12}-e_{22})(e_{13}-e_{23})(e_{12}-e_{32})(e_{16}-e_{36})+4d(e_{11}-e_{21})^2(e_{13}-e_{33})(e_{16}-e_{36})+4d(e_{12}-e_{22})^2(e_{13}-e_{33})(e_{16}-e_{36})-4d^3(e_{11}-e_{21})(e_{15}-e_{25})(e_{14}-e_{34})(e_{16}-e_{36})-4d^3(e_{11}-e_{21})(e_{16}-e_{26})(e_{16}-e_{36})(e_{14}-e_{34})+d^3(e_{11}-e_{21})(e_{14}-e_{24})(e_{16}-e_{36})^2-4(e_{12}-e_{22})(e_{11}-e_{21})(e_{11}-e_{31})(e_{16}-e_{36})-4d^3(e_{14}-e_{24})(e_{15}-e_{25})(e_{11}-e_{31})(e_{16}-e_{36})-4d(e_{14}-e_{24})(e_{16}-e_{26})(e_{11}-e_{31})(e_{16}-e_{36})-4(e_{12}-e_{22})(e_{13}-e_{23})(e_{12}-e_{32})(e_{16}-e_{36})+4(e_{11}-e_{21})^2(e_{13}-e_{33})(e_{16}-e_{36})-4d^2(e_{11}-e_{21})(e_{15}-e_{25})(e_{14}-e_{34})(e_{16}-e_{36})-4d(e_{11}-e_{21})(e_{16}-e_{26})(e_{14}-e_{34})(e_{16}-e_{36})+8d^2(e_{11}-e_{21})(e_{14}-e_{24})(e_{16}-e_{36})^2+4d(e_{11}-e_{21})(e_{14}-e_{24})(e_{16}-e_{36})^2$

$\lambda_{29}=-(e_{11}-e_{21})^2(e_{11}-e_{31})^2+d^2(e_{15}-e_{25})^2(e_{11}-e_{31})^2+2d(e_{15}-e_{25}(e_{16}-e_{16})(e_{11}-e_{31})^2+(e_{16}-e_{26})^2(e_{11}-e_{31})^2+2(e_{11}-e_{21})(e_{12}-e_{22})(e_{11}-e_{31})(e_{12}-e_{32})-(e_{11}-e_{21})^2(e_{12}-e_{32})^2+d^2(e_{15}-e_{25})^2(e_{12}-e_{32})^2d(e_{15}-e_{25})(e_{16}-e_{26})(e_{12}-e_{32})^2-2d^2(e_{11}-e_{21})(e_{15}-e_{25})(e_{11}-e_{31})(e_{16}-e_{36})-2d(e_{11}-e_{21})(e_{16}-e_{26})(e_{11}-e_{31})(e_{16}-e_{36})-2d^2(e_{12}-e_{22})(e_{15}-e_{25})(e_{12}-e_{32})(e_{16}-e_{36})-2d(e_{12}-e_{22})(e_{16}-e_{26})(e_{12}-e_{32})(e_{16}-e_{36})+d^2(e_{11}-e_{21})^2(e_{16}-e_{36})^2-2d(e_{11}-e_{21})(e_{15}-e_{25})(e_{11}-e_{31})(e_{16}-e_{36})-2(e_{11}-e_{21})(e_{16}-e_{26})(e_{11}-e_{41})(e_{16}-e_{36})2d(e_{12}-e_{22})(e_{15}-e_{25})(e_{12}-e_{32})(e_{16}-e_{36})-2(e_{12}-e_{22})(e_{12}-e_{32})(e_{16}-e_{36})+2d(e_{11}-e_{21})^2(e_{16}-e_{36})^2+2d(e_{12}-e_{22})^2(e_{16}-e_{6})^2+(e_{11}-e_{21})^2(e_{16}-e_{36})^2+(e_{12}-e_{22})^2(e_{16}-e_{36})^2$

Vita

Zhe Su was born in Chifeng, China to the parents of Weifeng Su and Chunhua He as their only child. He received his high school diploma from Chifeng No. 2 High School in 2011. After graduation he headed to Beijing Forestry University to study Automation. He received his B. S degree in 2015. It were these four meaningful years of study and internship experience in robotics industry that raised his interest in Robotics and Engineering. The desire of gaining more knowledge in robotics had driven him into continuing his education. He was admitted to the Department of Mechanical, Aerospace and Biomedical Engineering at the University Of Tennessee Knoxville as a Master's student in 2015 and he is expecting his graduation late 2018 or mid 2019. He is not looking for a chance to pursuit a Ph. D degree.